University of Alberta

Two New Approaches to Toughness Characterization of Polyethylene
- Case Studies on Low-Density Polyethylene and Ultra-High-Molecular-Weight Polyethylene

by

Wenrui Cao

A thesis submitted to the Faculty of Graduate Studies and Research
in partial fulfillment of the requirements for the degree of

Master of Science

Department of Mechanical Engineering

Fall 2011
Edmonton, Alberta

ABSTRACT

A new mechanistic approach is applied to characterizing toughness of low-density polyethylene (LDPE) in ductile fracture, introduced in double-edge-notched tensile (DENT) test. Three mechanisms were involved in the new approach, i.e. fracture surface formation, necking and shear plastic deformation. This is different from the original essential work of fracture (EWF) method, as the latter does not consider the shear plastic deformation. The specific energy density for the fracture surface formation, determined from the new approach, was found to be about 12% higher than that from the original EWF method, and the specific energy density for necking is close to that determined from simple tensile test. The closeness of specific energy density for necking between DENT and simple tensile tests provides some support to validity of the new approach in characterizing fracture behavior of polyethylene when accompanied by large plastic deformation and necking. Ultra-high-molecular-weight polyethylene (UHMWPE) was also characterized using DENT test. However, it was found that its fracture behavior cannot be described using the original EWF method, and since necking does not occur, nor by the new mechanistic approach. As a result, a modified EWF method was developed. To justify validity of the modified EWF method, a formulation of energy balance equation was established, from which a nonlinear trend line was used to determine the fracture toughness. This study indicates that the original EWF method cannot be used to deal with the

involvement of a significant amount of plastic deformation involved in the fracture process, for characterizing fracture behavior of UHMWPE.

ACKNOWLEDGEMENTS

I am particularly indebted to my supervisor Dr. P.-Y. Ben Jar for the guidance and financial support throughout this study.

I also would like to thank Ms. Tuula Hilvo for her consistent technical supports, help in the lab and some valuable discussions.

Appreciation is extended to group members of the Failure Analysis and Materials Evaluation Lab, Souvenir Muhammad and Tsegay Belay, for their friendship and positive group environment.

Special thanks to my best friend Jian Zhang for his help, suggestion and encouragement in writing the thesis.

Finally, gratitude is given to my parents, Yongqing Cao and Bo Wang, for their concerns and support throughout my study.

TABLE OF CONTENT

LIST OF TABLES

LIST OF FIGURES

LIST OF ABBREVIATIONS AND SYMBOLS

A	fracture surface area
ABS	acrylonitrile-butadiene-styrene
A_n	cross-sectional areas after the neck
A_0	original cross-sectional area
DCNT	deep-center-notched tension
DENT	double-edge-notched tensile
E	Young's modulus
Eu	total energy consumed for plastic deformation during the neck formation
EWF	essential work of fracture
F	load
F_c	load at the beginning of neck propagation stage
F_{max}	maximum load
H	height for each strip in the original plastic zone
HDPE	high-density polyethylene
H_0	height of the original ligament region that later undergoes plastic deformation
h	height of OPDZ
h_n	height of active deformation zone
h_0	original height of active deformation zone
IFPZ	inner fracture process zone
J_c	value for crack initiation
J_R	resistance to crack growth
L	length of specimen in simple tensile test

LDPE	low-density polyethylene
L_0	original length of specimen in simple tensile test
l	ligament length
l_p	horizontal diagonal symmetric quadrilateral zone
l_0	original ligament length
l_1	original gauge length
m	unloading stiffness
m_c	stiffness at the beginning of neck propagation stage
OPDZ	outer plastic deformation zone
PE	polyethylene
R_p	size of OPDZ
s	half of the remaining ligament length
T	specimen thickness
Tg	glass transition temperature
t	thickness of specimen
t_n	final thickness
$t(s)$	time as a function of s
t_0	original thickness
t_1	half of thickness in the middle of the ligament section
t_2	half of thickness at both ends of the ligament section
U	strain energy
UHMWPE	ultra-high-molecular-weight polyethylene
V_c	crack growth speed value
V_n	volume of the necking zone
V_s	volume of shear plastic deformation zone

V_{δ}	cross-head speed for the DENT test
B	width of the specimen
W_e	essential work of fracture
W_f	total work of fracture
W_p	non-essential work of fracture
w	width of specimen in simple tensile test
w_e	specific essential work of fracture
w_f	specific total work of fracture
w_p	specific work of plastic deformation fracture
w_n	necking energy density
$w_{p,n}$	specific energy for necking
$w_{p,s}$	specific energy for shear plastic deformation
w_0	original width of specimen in simple tensile test
x_b	extension of specimen at failure
x_p	plastic contribution to the extension
x_0	crack open displacement
β	shape factor representing the relationship between h and l
β_h	parameter, along with h_0 for characterizing neck dimension
Δa	crack extension
δ	displacement of DENT test
δ_c	displacement at the commencement of the neck propagation stage
δ_{fract}	displacement at fracture
δ_1	displacement at the beginning of the necking process
δ_2	displacement at which the cross-sectional area of the specimen stop shrinking

ε	true strain
σ_y	strength

Chapter 1 Introduction

A polymer is made of large molecules each of which consists of repeating structural units that are connected by covalent bonds. The earliest work in polymer science started from early 19th century. Till today, due to the advantages of light weight, good corrosion resistance and low cost, polymers have become the most important commercial material nearly everywhere in our daily life, such as construction, automotive, aerospace, household appliances, etc.

Polyethylene (PE) is one of the commodity thermoplastics, which has ethylene as the monomer, hence the name "polyethylene." It has several categories, based mostly on the density and branching. Due to variations such as the extent and type of branching, the crystal structure and the molecular weight, mechanical properties among those categories can be very different. Among those, three most well-known types of polyethylene are high-density polyethylene (HDPE), low-density polyethylene (LDPE) and ultra-high-molecular-weight polyethylene (UHMWPE).

Because of the wide use of polymers, the mechanical properties are of great importance. Usually, the fracture process can be categorized by the fracture behavior, i.e. brittle or ductile, based on the amount of deformation involved in the process. For the brittle fracture, only very limited or no plastic deformation is involved. While for ductile fracture, the polymer can undergo significant plastic deformation, which occurs more often in plane stress condition than in plane strain condition.

Nowadays, many researches are using the concept of essential work of fracture (EWF) to characterize the fracture toughness, mostly based on data from double-edge-notched tensile (DENT) test. For polymers like LDPE, very ductile deformation occurs during the process (referred to as the neck propagation stage) [1]. On the other hand, UHMWPE shows a relatively small amount of ductile deformation before fracture [2].

Focus of this study is to determine the fracture toughness of LDPE under plane-stress condition using a new mechanistic approach for the opening mode of fracture. Different from the EWF method, the new approach considers mechanism of shear plastic deformation. To justify results from the new mechanistic approach, results from a simple tensile test are compared with the energy for the neck formation in the DENT test. For UHMWPE, since necking does not occur, a modified EWF method has been developed to determine its toughness.

1.1 Literature Review

1.1.1 EWF concept

Broberg [3] is the first to propose the concept of EWF. He divided the total work of fracture into two parts: the dissipative work in outer "plastic" zone and essential work in the inner autonomous region which is also called fracture process zone. He also pointed out that the latter is a material property known as toughness [4, 5].

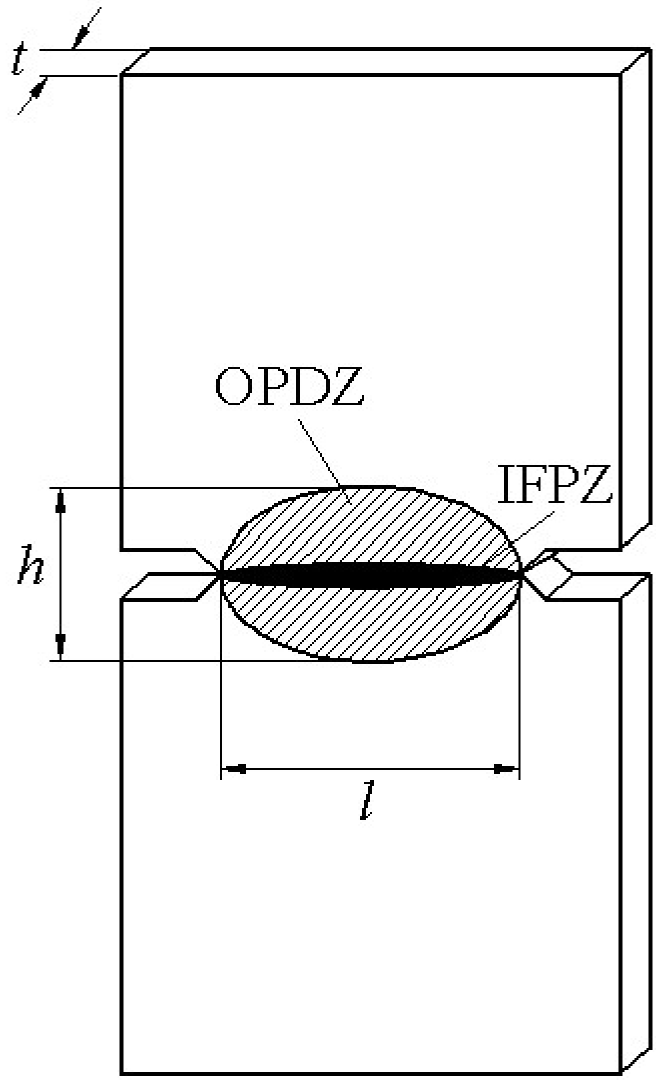

Fig.1-1 Schematic diagram showing the fracture regions involved in the fracture process: inner fracture process zone (IFPZ), and outer process dissipation zone (OPDZ).

Cotterell and Reddel [6], based on the EWF concept, were the first to develop a method for determining the property of thin, ductile metals. Mai et al. [7-9] extended the application of the EWF method to polymers. As mentioned above, the total work of fracture (W_f) can be partitioned into two parts: the essential work of fracture (W_e) which is necessary in forming the crack surfaces in the inner fracture process zone (IFPZ) and the non-essential (plastic) work (W_p) which is not necessary for forming the crack surfaces in the outer plastic deformation zone (OPDZ) surrounding IFPZ as shown in Fig. 1-1.

The relationship between the above three parameters can be given by Equation (1-1)

$$W_f = W_e + W_p \tag{1-1}$$

As defined, W_e is proportional to the ligament length l and thickness t. On the other hand, OPDZ is an elliptical zone determined by the height h of the corresponding zone, l and t as shown in Fig.1-1. Therefore, Equation (1-1) can be rewritten into Equations (1-2) and (1-3) as:

$$W_f = w_f\, lt = w_e\, lt + \beta w_p l^2 t \tag{1-2}$$

where w_e is the specific essential work of fracture, w_p the specific work of plastic deformation fracture, and β a shape factor representing the relationship between h and l. After normalizing by the product of l and t to both sides of Equation (1-2), the following equation can be found:

$$w_f = w_e + \beta w_p l \tag{1-3}$$

Based on Equation (1-3), w_e can be determined by plotting w_f as a function of l in which βw_p is the slope of the plot. This method has been widely used to determine w_e which is the intercept on the vertical axis of the plot [9-19], as shown in Fig.1-2.

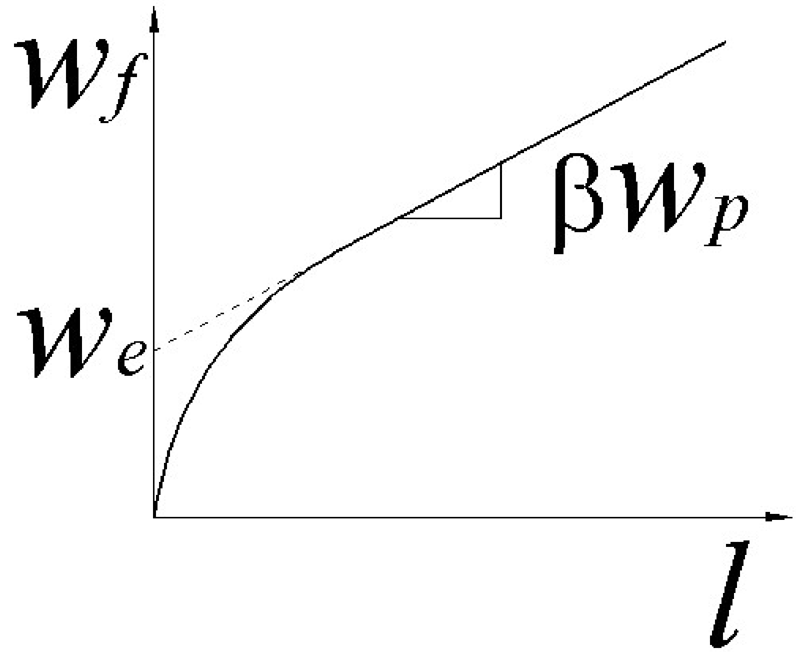

Fig.1-2 Plot of specific total work of fracture w_f , versus ligament length l.

The main concept of the EWF method is energy partitioning. Mai and Cotterell [9] considered the elastic energy during the fracture procedure. They also defined the crack initiation by inspection. Karger-Kocsis [20] proposed a partition scheme based on the slope of the load-displacement curve. However, this concept does not always work. Vu-Khanh [21] found that the curve of w_f vs. l yields a negative intercept (w_e) or negative slope (βw_p) [22]. This may be because of the transition of stress state from plane-stress to plane-strain fracture. Another reason may be the way of partitioning the total energy; Jar et al. [23] showed that besides necking, the shear plastic deformation should also be considered in the fracture process. In this new approach, the specific work of plastic deformation, w_p, is divided into two parts, $w_{p,n}$ and $w_{p,s}$ which represent the energy density for necking and shear deformation, respectively. In addition, a comparison between the original EWF method and the new approach was given to prove that, the new approach is applicable to ductile fracture in polymers like polyethylene.

The original EWF method was developed for a fracture process that meets the following conditions:

(i) The material in the ligament region yields completely before crack growth commences, and

(ii) Only the ligament region yields.

To guarantee that the above requirements are satisfied, the ligament length should meet the condition set out by Equation (1-4) [9, 24]:

$$(3\text{-}5)t_0 \leqslant l \leqslant min(B/3 \text{ or } 2R_p) \quad (1\text{-}4)$$

where B is width of the specimen and R_p the size of OPDZ. R_p can be estimated using Young's modulus E and stress σ_y as [24]:

$$2R_p = \frac{1}{\pi}\left(\frac{Ew_e}{\sigma_y^2}\right) \quad (1\text{-}5)$$

The value for the left hand-side of Equation (1-4) is to make sure that the specimen fractures in the plane-stress condition. If l is smaller than the lower bound, the deformation state will fall into transition from plane-stress to plane-strain condition [9], which will result in a nonlinear relationship between w_f and l.

1.1.2 EWF under mode Ⅰ, Ⅱ and Ⅲ loading

Crack propagation can be summarized into three modes, known as mode I (or the opening mode, generated by a tensile load normal to the plane of the crack); mode II (or the sliding mode, generated by a shear load acting parallel to the plane of the crack and perpendicular to the crack front); and mode III (or the tearing mode, generated by a shear load acting parallel to both the plane of the crack and the crack front).

Most of the studies on fracture are under mode I loading. Until now, only very limited papers have tested material like LDPE, as most of the studies were concerned about high-density polyethylene (HDPE). Chan and Williams [25] used both DENT and single-edge-notched tensile (SENT) tests to investigate the effects of specimen width and material types on linear low-density polyethylene (LLDPE). Casellas et al. [1] tested LDPE under different temperature using data collected from DENT tests, to estimate how annealing/quenching affects w_e via crack opening displacement (COD) method. The testing results of LDPE from Pegoretti [26] and Wu [27] match each other very well. The former used the test speed of 20 mm/min; while the latter used 100 mm/min. They both got w_e values in the range of 35-50 KJ/m^2 and βw_p around 9 MJ/m^3.

By comparing test results from polymers such as HDPE, polypropylene, and polyvinyl chloride [28-45], it has been concluded that w_e usually increases with the increase of deformation rate but decreases with the increase of temperature; while the opposite trend holds for βw_p. In addition, it was found that βw_p reaches maximum at a temperature slightly above the glass transition temperature of the polymers [46].

All of the above studies are under mode Ⅰ and static loading, for mode Ⅱ loading was checked only by a few researchers. Kwon and Jar [47, 48] found that for poly (acrylonitrile-butadiene-styrene) (ABS), the specific work of fracture in mode Ⅱ was independent of ligament length of the specimen and the corresponding deformation rate was two times of that in mode Ⅰ loading at the same test speed (2.5 mm/min). Also, w_e value for mode Ⅱ is about 2.5 times of the corresponding value for mode Ⅰ.

Rivlin and Thomas [49] developed a method to determine the tear resistance of rubber. Later, Wong [50] and Hashemi [51] applied the theory in estimating the toughness of polymers. In their studies, the fracture zone can be divided into two parts: zone A representing the triangular area under the crack and zone B along the height of plastic zone having a constant width.

1.1.3 Comparison between different tests and other fracture mechanics parameters

So far, only a few of studies have compared [52] the EWF parameters under mode Ⅰ and mode Ⅲ loading. Kwon and Jar [47, 48] are the only researchers who have done the comparison between mode Ⅰ and mode Ⅱ. Till today, no one has done the comparison among all three modes.

Different from the scarce in comparison between three types of loading modes, some comparisons were made between parameters of the EWF method and other fracture mechanics parameters, such as crack tip opening displacement (CTOD) and *J*-integral. Hashemi and O'Brien [53-56] used the theory of CTOD to estimate w_e. The method is to plot the extension of specimen at failure (x_b) versus the ligament length (l), as shown by Equation (1-6):

$$x_b = x_0 + x_p\, l \tag{1-6}$$

where x_b is determined from load-displacement curves, x_0 CTOD and x_p contribution of plastic deformation to the extension. In addition, w_e can be determined from Equation (1-7):

$$w_e = \sigma_y\, x_0 \tag{1-7}$$

where σ_y is the yield strength for the corresponding polymer.

The other widely used parameter is *J*-integral, which represents the resistance (R) curve. *J*-integral and EWF are suggested to be similar to each other, because the resistance to crack growth (J_R) is also a linear function (Equation 1-8) of crack extension (Δa), just like w_f vs. l.

$$J_R = J_C + \frac{dJ}{da} \cdot \Delta a \tag{1-8}$$

where J_c is the *J*-integral value for crack initiation and dJ/da the potential energy release rate per unit thickness.

It has been proven by Mai et al. [10] through DENT and deep-center-notched tension (DCNT) tests that Equation (1-9) holds:

$$w_f = \frac{l}{4}\frac{dJ}{da} \tag{1-9}$$

By comparison with Equation (1-3), accordingly, $w_e = J_c$ and $\beta w_p = \frac{l}{4}\frac{dJ}{da}$.

In practice, it is not easy to determine the crack extension (Δa) and the J-integral value when large deformation occurs. Therefore, the EWF method becomes more popular than the J-integral method.

There are some applications based on the EWF method, such as the use of EWF method [57] to estimate the life expectation of HDPE pipe, and capacity limit of the fluid-filled PE containers [58]. Note that in this thesis, all the test results were obtained from DENT test.

1.2 Objective and scope of the study

The EWF method is very popular for obtaining fracture toughness. The results can also reflect work needed for different mechanisms. By plotting the total work of fracture W_f vs. the ligament length l, the essential work of fracture w_e and the slope (βw_p, the non-essential part of the work of fracture) can be calculated. But for some very ductile polymers, application of the EWF method may result in negative w_e or βw_p values, which is against the reality. By inspection of the necking zone in the specimens, Jar et al. [20] proposed a new approach based on three deformation mechanisms, instead of two in the original EWF method. They demonstrated the new approach using HDPE. This thesis extends this concept to

LDPE. In addition, UHMWPE, in which the necking behavior is not as significant as HDPE or LDPE, is included in the study. Both LDPE and UHMWPE were fractured in the plane-stress condition, to which the original EWF method cannot be applied. For UHMWPE, a modified EWF method is proposed, and for LDPE the mechanistic approach.

The overall objective of this thesis is to determine the material properties of LDPE and UHMWPE, and compare the results with those from the original EWF method.

In this thesis, Chapter 1 introduces the background information of the study. Chapter 2 is mainly about determination of toughness for LDPE using the new approach. Chapter 3 is focused on whether the original EWF method can be applied for the determination of material properties of UHMWPE. In Chapter 4, the general conclusions as well as the recommendations for the future study are given. Note that this thesis adopts the paper format. Therefore, some information is repeated in each chapter.

References

[1] Casellas JJ, Frontini PM, Carella M. Fracture characterization of low-density polyethylene by the essential work of fracture: changes induced by thermal treatments and testing temperature. J Appl Polym Sci 1999; 74: 781-96.

[2] Ching ECY, Poon WKY, Li RKY, Mai YW. Effect of strain rate on the fracture toughness of some ductile polymers using the essential work of fracture (EWF) approach. Polym Engng Sci 2000; 40: 2558-68.

[3] Broberg KB. Critical review of some theories in fracture mechanics. Int J Fracture 1968; 4:11-8.

[4] Broberg KB. Crack–growth criteria and non-linear fracture mechanics. J Mech Phys Solids 1971;19:407-18.

[5] Briberg KB. On stable crack growth. J Mech Phys Solids 1975; 23: 215-37.

[6] Cotterell B, Reddel JK. The essential work of plane stress ductile fracture. J Int Fract 1977; 13: 267-277.

[7] Karger-Kocsis J. Microstructual and molecular dependence of the work of fracture parameters in semicrystalline and amorphous polymer systems. In: Williams G, Pavan A, editors. Fracture of polymers, composites and adhesives, Vol 27. Oxford: Elsevier and ESIS Publ; 2000. P. 213-30.

[8] Mai Y-W, Wong S-C, Chen X-H. Application of fracture mechanics for characterization of toughness of polymer blends. In: Paul DR, Bucknall CB,

editors. Polymer blends: formulations and performance, Vol 2. NewYork: Wiley; 2000. P. 17-58.

[9] Mai YW, Cotterell B. On the essential work of ductile fracture in polymers. Int J Fracture 1986; 32: 105-25.

[10] Mai YW, Powell P. Essential work of fracture and J-integral measurements for ductile polymers. J Polym Sci Part B Polum Phys 1991; 29: 785-93.

[11] Mai YW, Cotterell B, Horlyck R, Vigna G. The essential work of plane stress ductile fracture of linear polyethylenes. Polym Engng Sci 1987; 27(11):804-9

[12] Peres F, Schon C. Application of the essential work of fracture method in ranking the performance in service of high-density polyethylene resins employed in pressure pipes. J Mater Sci 2008; 43(6): 1844-50.

[13] Kwon HJ, Jar PYB. Application of essential work of fracture concept to toughness characterization of high-density polyethylene. Polym Engng Sci 2007; 47(9): 804-9.

[14] Maspoch ML, Ferrer D, Gordillo A. Effect of the specimen dimensions and the test speed on the fracture toughness of iPP by the essential work of fracture (EWF) method. J Appl Polym Sci 1999; 73(2): 177-87.

[15] Hashemi S. Determination of the fracture toughness of polyethylene terephthalate (PBT) film by the essential work method: effect of specimen size and geometry. Polym Engng Sci 2000; 40(3): 798-808.

[16] Levita G, Parisi L, Marchetti A. Effect of thickness on the specific essential work of fracture of rigid PVC. Polym Engng Sci 1996; 36(20): 2534-41.

[17] Hashemi S. Work of fracture of PBT/PC blend: effect of specimen size, geometry, and rate of testing. Polym Engng Sci 1997; 37(5): 912-21.

[18] Wu J, Mai YW. The essential fracture work concept for toughness measurement of ductile polymers. Polym Engng Sci 1996; 36(18): 2275-88.

[19] Ferrer-Balas D, Maspocha ML, Martinez AB, Ching E, Li RKY, Mai YW. Fracture behavior of polypropylene films at different temperatures: assessment of the EWF parameters. Polymer 2001; 42: 2665-74.

[20] Karger-Kocsis J. For what kind of polymer is the toughness assessment by the essential work concept straightforward? Polym Bull 1996; 37: 119-26.

[21] Vu-Khanh T. Impact fracture characterization of polymer with ductile behavior. Theor Appl Fract Mech 1994; 21: 83-90.

[22] Bernal CR, Frontini PM. Determination of fracture-toughness in rubber-modified glassy-polymers under impact conditions. Polym Eng Sci 1995; 35: 1705-12.

[23] Jar PYB, Adianto R. Determination of plane-strain fracture toughness of polyethylene copolymer based on the concept of essential work of fracture. Polym Engng Sci 2010; 50: 530-5.

[24] Mai YW, Cotterell B. The essential work for tearing of ductile metals. Int J Fracture 1984; 24: 229-36.

[25] Chan WYF, Williams JG. Determination of the fracture-toughness of polymeric films by the essential work method. Polymer 1994; 35:1666-72.

[26] Pegoretti A, Castellani L, Franchini L, Mariani P, Penati A. On the essential work of fracture of linear low-density-polyethylene. I. Precision of the testing method. Eng Fract Mech 2009; 76: 2788-98.

[27] Wu JS, Mai YW. The essential fracture work concept for toughness measurement of ductile polymers. Polym Eng Sci 1996; 36: 2275-88.

[28] Supatham P, Tabtiang A, Venables RA. Plane stress fracture toughness of partially miscible, high-density polyethylene/poly (ethylene-co-1-octene) blends. Polym-Plast Technol Eng 2005; 44: 363-79.

[29] Gamez-Perez J, Santana OO, Gordillo A, Maspoch ML. Evaluation of the fracture behavior of multilayered polypropylene sheets obtained by coextrusion. Polym Engng Sci 2007; 47: 1365-72.

[30] Na B, Lv RH. Effect of cavitation on the plastic deformation and failure of isotactic polypropylene. J Appl Polym Sci 2007; 105: 3274-9.

[31] Mohanraj J, Chapleau N, Ajji A, Duckett RA, Ward IM. Fracture behavior of die-drawn toughened polypropylenes. J Appl Polym Sci 2003; 88: 1336-45.

[32] Karger-Kocsis J, Varga J. Effects of beta-alpha transformation on the static and dynamic tensile behavior of isotactic polypropylene. J Appl Polym Sci 1996; 63: 291-300.

[33] Wallner GM, Major A, Maier G, Lang RW. Influence of annealing on the fracture behavior of 200 μm thick alpha-PVDF films. Adv Eng Mater 2006; 8: 1140-5.

[34] Wallner GM, Major Z, Maier GA. Lang RW. Fracture analysis of annealed PVDF films. Polym Test 2008; 27: 392-402.

[35] Levita G, Parisi L, Marchetti A, Bartolommei L. Effects of thickness on the specific essential work of fracture of rigid PVC. Polym Engng Sci 1996; 36: 2534-41.

[36] Gong G, Xie BN, Yang W, Li ZM, Lai SM, Yang MB. Plastic deformation behavior of polypropylene/calcium carbonate composites with and without maleic anhydride grafted polypropylene incorporated using the essential work of fracture method. Polym Test 2006; 25: 98-106.

[37] Gong G, Xie BN, Yang W, Li ZM, Zhang WQ, Yang MB. Essential work of fracture (EWF) analysis for polypropylene grafted with maleic anhydride modified polypropylene/calcium carbonate composites. Polym Test 2005; 24: 410-7.

[38] Tjong SC, Xu SA, Li RKY, Mai YW. Fracture characteristics of short glass fibre/maleated styrene-ethylene-butylene-styrene/polypropylene hybrid composite. Polym Int 2002; 51: 1248-55.

[39] Tjong SC, Xu SA, Li RKY, Mai YW. Tensile deformation mechanisms of polypropylene/elastomer blends reinforced with short glass fiber. J Appl Polym Sci 2003; 87: 441-51.

[40] Li B, Gong G, Xie BH, Yang W, Yang MB, Lai SM. Fracture behavior of polypropylene sheets filled with epoxidized natural rubber (ENR) treated coal gangue poeder. J Mater Sci 2007; 31: 1—7.

[41] Arencon D, Velasco JI, Realinho V, Antunes M, Maspoch ML. Essential work of fracture analysis of glass micro sphere-filled polypropylene and polypropylene/poly (ethylene terephthalateco-isophthalate) blend-matrix composites. Polym Test 2007; 26: 761-9.

[42] Kwon JA, Truss RW. The work of fracture in uniaxial and biaxial oriented unplasticised polyvinylchloride pipes. Eng Fract Mech 2002; 69: 605-16.

[43] Lau SW, Truss RW. The essential work of fracture through the wall of a uPVC pipe. J Mater Sci 2002; 37: 1115-9.

[44] Whittle AJ, Burford RP, Hoffman MJ. Assessment of strength and toughness of modified PVC pipes. Plast Rubber Compos 2001; 30: 434-40.

[45] Yokoyama Y, Ricco T. Toughening of polypropylene by different elastomeric systems. Polymer 1998; 39: 3675-81.

[46] Mohanraj J, Chapleau N, Ajji A, Duckett RA, Ward IM. Fracture behavior of die-drawn toughened polypropylenes. J Appl Polym Sci 2003; 88: 1336-45.

[47] Kwon HJ, Jar PYB. Fracture toughness of polymers in shear mode. Polymer 2005; 46: 12480-92.

[48] Kwon HJ, Jar PYB. Toughness of high-density polyethylene in shear fracture. Int J Fracture 2007; 145: 123-33.

[49] Rivlin RS, Thomas AG. Rupture of rubber. I. Characteristic energy for tearing. J Polym Sci 1953; 10: 291-318.

[50] Wong JSS, Ferrer-Balas D, Li RKY, Mai YW, Maspoch ML. Sue HJ. On tearing of ductile polymer films using the essential work of fracture (EWF) method. Acta Mater 2003; 51: 4929-38.

[51] Hashemi S. Ductile frature of polymer films. Plast Rubber Compos 1993; 20: 229-37.

[52] Martinez AB, Gamez-Perez J, Sanchez-Soto M, Velasco JI, Santana OO, Maspoch ML. The essential work of fracture (EWF) method – analyzing the post-yielding fracture mechanics of polymers. Eng Fail Anal 2009; 16: 2604-17.

[53] Hashemi S, Obrien D. The essential work of plane-stress ductile fracture of poly (ether-ether ketone) thermoplastic. J Mater Sci 1993; 28: 3977-82.

[54] Hashemi S. Fracture toughness evaluation of ductile polymeric films. J Mater Sci 1997; 32: 1563-73.

[55] Mouzakis DE, Karger-Kocsis J, Moskala EJ. Interrelation between energy partitioned work of fracture parameters and the crack tip opening displacement in amorphous polyester films. J Mater Sci Lett 2000; 19: 1615-9.

[56] Wells AA. Application of fracture mechanics at and beyond general yielding. Br Weld J 1963; 10: 563-70.

[57] Peres FM, Schon CG. Application of the essential work of fracture method in ranking the performance in service of high-density polyethylene resins employed in pressure pipes. J Mater Sci 2008; 43: 1844-50.

[58] Karac A, Ivankovic A. Modeling the drop impact behavior of fluid filled polyethylene containers. In: Blackman BRK, Pavan A, Williams JG, editors. Fracture of polymers, composites and adhesives II, Vol 32. Oxford: Elsevier Ltd. and ESIS; 2003. p. 253-64.

Chapter 2 Evaluation of Toughness for Low-Density Polyethylene based on the New Mechanistic Approach

2.1 Introduction

Broberg [1] is the first to propose the concept of essential work of fracture (EWF) method. He divided the total work of fracture into two parts: the dissipative work in the outer "plastic" zone and the essential work in the inner autonomous zone which is also called the fracture process zone. He also pointed out that the latter is a material property known as toughness [2, 3].

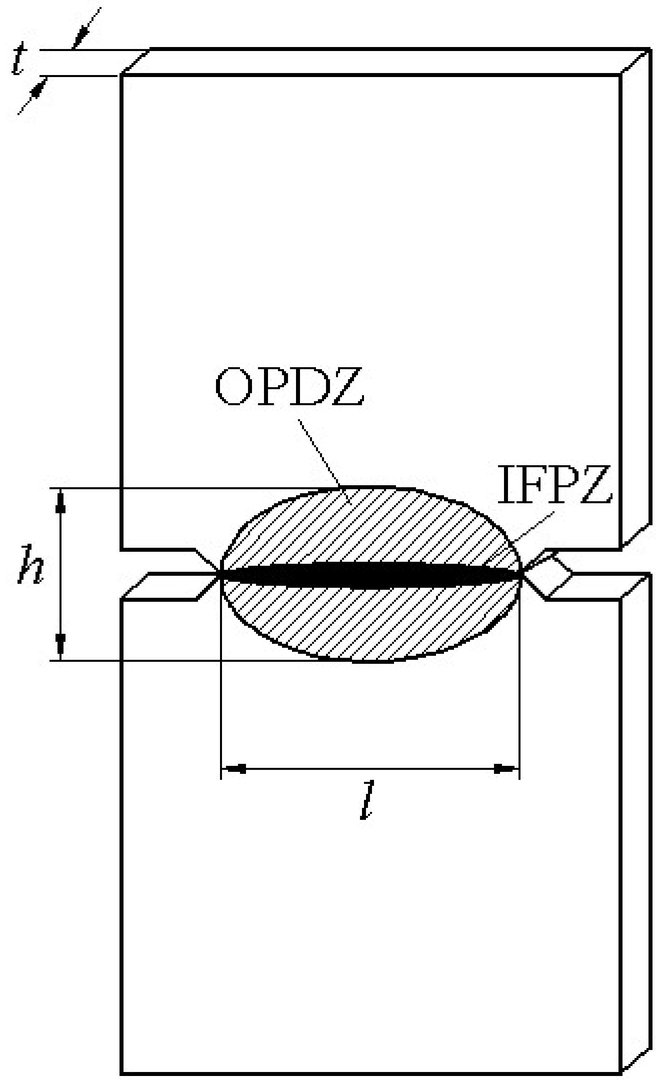

Fig.2-1 Schematic diagram showing the regions involved in the fracture process: inner fracture process zone (IFPZ), and outer plastic deformation zone (OPDZ).

Cotterell and Reddel [4], based on the EWF concept, were the first to develop a method for determining the property of thin, ductile metals. Mai et al. [5-7] extended the application of the EWF method to polymers. As mentioned before, the total work of fracture (W_f) can be partitioned into two parts: the essential work of fracture (W_e) in the inner fracture process zone (IFPZ) and the non-essential (plastic) work of fracture in the outer plastic deformation zone (OPDZ) surrounding IFPZ (W_p), as shown in Fig. 2-1.

The relationship between the above three parameters can be given by Equation (2-1)

$$W_f = W_e + W_p \tag{2-1}$$

As defined, W_e is proportional to the ligament length l and thickness t. On the other hand, OPDZ is an elliptical zone determined by the height h of the corresponding zone, ligament length l and thickness t, as shown in Fig.2-1. Therefore, Equation (2-1) can be rewritten as Equations (2-2) and (2-3):

$$W_f = w_f\, lt = w_e\, lt + \beta w_p l^2 t \tag{2-2}$$

where w_e is specific essential work of fracture, w_p specific plastic deformation energy, and β a shape factor representing the relationship between h and l. After normalizing both sides of Equation (2-2) using lt, the following equation can be obtained:

$$w_f = w_e + \beta w_p l \tag{2-3}$$

Based on Equation (2-3), w_e can be determined by plotting w_f as a function of l in which βw_p is the slope of the plot. This method has been widely used to determine w_e which is the intercept on the vertical axis [5, 6, 7-15], as shown in Fig.2-2.

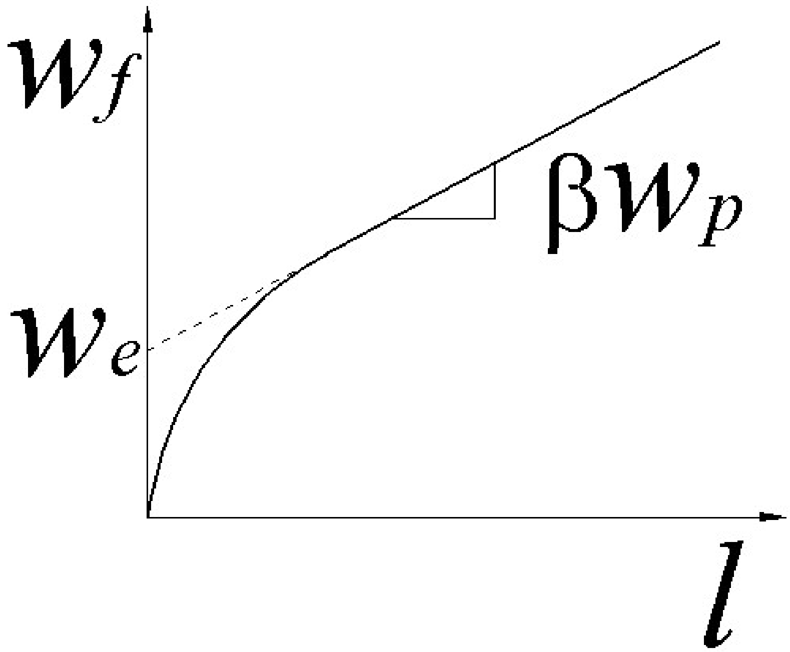

Fig.2-2 Plot of specific total work of fracture, W_f versus ligament length *l*.

The main concept of the EWF method is energy partitioning. Mai and Cotterell [5] considered the elastic energy during the fracture process. Basically, their model separates the non-elastic energy consumption into two parts, one for IFPZ and the other for OPDZ, with the assumption that shape of the OPDZ does not depend on the specimen geometry and loading condition. Karger-Kocsis [16] modified the original approach by further dividing W_f but did not take into account the elastic energy. His energy partition method is based on the slope of the load-displacement curve. However, this concept does not always work. Vu-Khanh [17] reported that the curve of w_f vs. l for high impact polystyrene yields a negative intercept (w_e) or negative slope (βw_p) [18] and concluded that the EWF method is not suitable for characterizing impact fracture toughness of polymers. This may be because due to the transition of stress state by increasing the loading rate, such as from plane stress to plane strain, shape of the OPDZ changes. It is believed that the negative intercept or negative slope may be caused by the way of partitioning the total energy, For example, Jar et al. [19] have shown that for high-density polyethylene (HDPE), besides necking mechanisms involved in the fracture process should include shear plastic deformation. In this new approach, the specific plastic work of fracture w_p is divided into two parts, $w_{p,n}$ and $w_{p,s}$ which correspond to the energy density for necking and that for shear deformation, respectively. In addition, a comparison between the original EWF method and the new approach for HDPE suggests that the latter is more suitable than the former for ductile fracture of polymers like polyethylene.

As mentioned in the previous chapter, applicability of the original EWF method is limited to the fracture behavior that occurs only after the whole ligament region has yielded, and the yielding is confined to the ligament region only.

To guarantee that the above requirements are satisfied, the ligament length should meet Equation (2-4) [4, 7]:

$$(3\text{-}5)t_0 \leqslant l \leqslant min(B/3 \ or \ 2R_p) \tag{2-4}$$

where B is width of the specimen, and R_p the size of OPDZ. R_p can be estimated using Young's modulus E and stress σ_y as:

$$2R_p = \frac{1}{\pi}\left(\frac{Ew_e}{\sigma_y^2}\right) \tag{2-5}$$

The lower bound of Equation (2-4) is to make sure that the specimen fractures in the plane-stress conditions. If l is smaller than the lower bound, the deformation state will fall into transition from plane stress to plane strain [7] which will result in the nonlinear relationship between w_f and l.

In this chapter, conditions for mechanical tests and description of the trend for the test results will be presented first. Then, mechanisms involved in the test based on the specimen fracture behavior will be identified. After that, w_e value will be determined using the new mechanistic approach. Values from the new approach will be compared with the corresponding values from the original EWF method. The last part of this chapter will be focused on the specific necking energy density, determined from the new mechanistic approach, and compared with the value from simple tensile test.

2.2 Experimental details

2.2.1 Materials

Low-density polyethylene (LDPE) is the first of the polyethylene family being developed for commercial applications, by Imperial Chemical Industries (ICI) in 1933. Despite competition from other polymers, LDPE is still regarded as one of the most important thermoplastics in commercial applications. Density of LDPE is in the range from 0.910 to 0.940 g/cm^3. It is inert to most chemicals at room temperature, except strong oxidizing agents and some solvents that can cause its swelling. LDPE can be exposed continuously at temperature up to 80°C, and for a short period up to 95°C. Its appearance varies from very translucent to nearly opaque. Although LDPE is breakable, it is commonly known to be flexible and tough.

Molecules of LDPE contain a large number of short and long chain branches, which makes them difficult to form a tightly-packed crystal structure. This is believed to result in low tensile strength but good ductility. It should be noted that the high degree of long-chain branching is desirable for processing molten LDPE, as it provides unique flow properties. Nowadays, LDPE is widely used for various applications, from rigid containers to plastic film such as plastic bags and sandwich wrap.

LDPE used in this study is provided by King Plastic Corporation, with density of 0.932 g/mm^3. It is a visco-elastic material, but at this stage, the visco-elastic behaviour is not considered.

2.2.2 Test set-up

In this study, Galbadini Quasar 100 universal testing machine was used to conduct double-edge-notched tensile (DENT) tests at a cross-head speed of 5 mm/min. A Nikon D-70 camera was used to record the deformation and fracture behavior during the whole fracture process at a rate of one photo per ten seconds. Those photos were used to measure the ligament length in order to determine the crack growth speed during the fracture process.

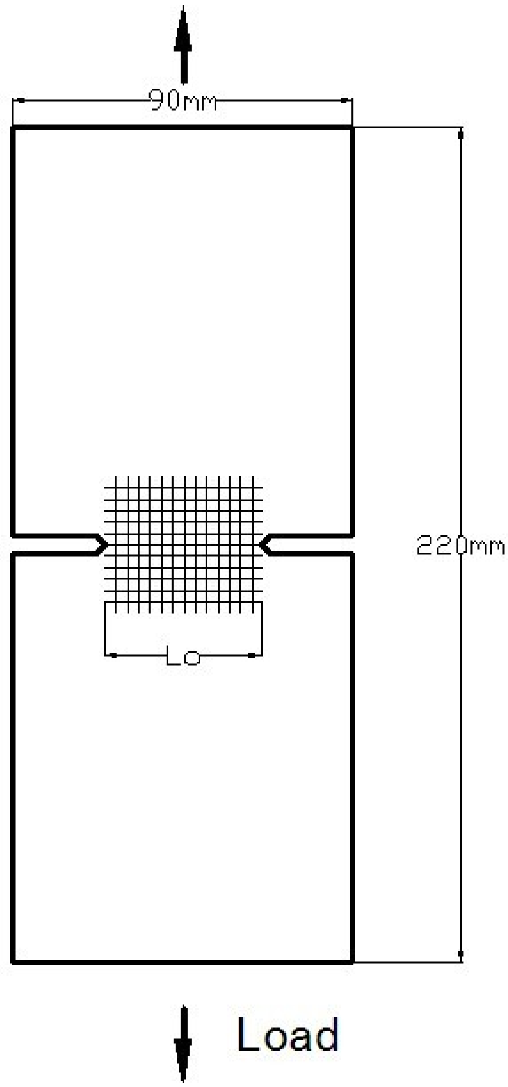

Fig.2-3 Schematic description of DENT specimens and mesh pattern introduced in the ligament section.

As shown in Fig. 2-3, specimen dimensions for the DENT test are 220 mm × 90 mm with nominal thickness 6.5 mm. Note that a rectangular mesh pattern was introduced in the ligament area of all specimens before the test, for which photographs taken during the test were used to measure the ligament contraction due to the neck development and crack growth.

Following the specification given in Equation (2-4), the original ligament length (l_0) of specimens used in this study is in the range from 20 to 34 mm at an increment of 2 mm. Two specimens were tested for each ligament length (except for $l_0 = 28$ mm, for which only one specimen was tested). Also, to avoid a blunt notch tip to inflate the w_e value [20], a very sharp tip was introduced prior to the tests using a fresh razor blade. Note that l_0 was measured between two sharp tips in each specimen using the software PHOTOSHOP.

2.3 Deformation and fracture behavior of LDPE in DENT test

Many polymers such as polyethylene can generate extensive necking in plane-stress fracture. Kwon and Jar [11] pointed out that the whole necking process can be divided into two stages: neck initiation and neck propagation. The neck growth in the first stage is along the ligament length direction, while in the second stage in the loading direction. The crack growth in the first stage (from the notch tip) is accompanied with ligament thickness reduction (from original thickness t_0 to the final thickness t_n). This represents a transition from plane-stain to plane-stress conditions. After that the ligament thickness would remain constant, and the neck growth becomes perpendicular to the ligament length, which is referred to as the neck propagation stage (the second stage). Note that, for determining fracture toughness in the plane-stress condition, the energy consumed during the first stage should not be considered.

To illustrate the fracture and deformation behavior of LDPE in DENT test, a typical load-displacement curve with snap shots of the ligament reduction are presented in Fig. 2-4. Fig. 2-4a shows the change of load-drop rate during the whole fracture process. The figure shows that the load-drop rate in the neck initiation stage (from the left vertical dash line at the maximum loading point to the right vertical dash line at the transition point) is higher than that in neck propagation stage (from right vertical dash line to the end of the curve). Note that the section of the curve for the neck propagation stage follows a linear relationship between load and displacement, except at the very end where a relative sharp load drop occurs.

Fig. 2-4b shows the top, front and side views of a DENT test specimen after the test. The top and side views show clearly that significant thickness reduction happened from the notch tip during the first stage, i.e. the neck initiation stage, while in the second stage, i.e. the neck propagation stage, this does not happen. In the neck propagation stage, the ligament thickness has been reduced significantly and remained nearly constant. Therefore, energy consumed for unit volume of neck development at the neck propagation stage can be considered as constant. In other words, the total amount of the non-essential part of energy consumption during this stage should be proportional to the neck volume developed at the neck propagation stage. Note that, based on the front view of Fig. 2-4b a symmetric quadrilateral zone of constant thickness can be outlined in the fractured specimen, with the horizontal diagonal equal to l_p that represents the total crack growth length at the neck propagation stage.

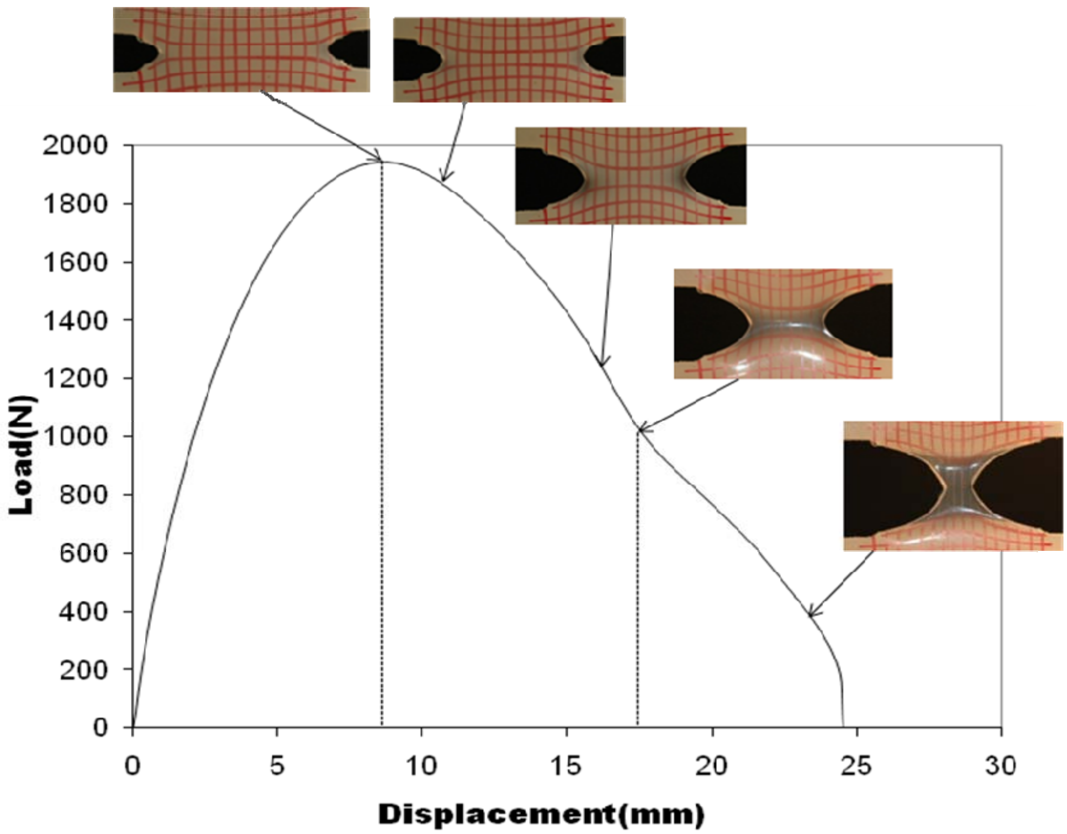

(a)

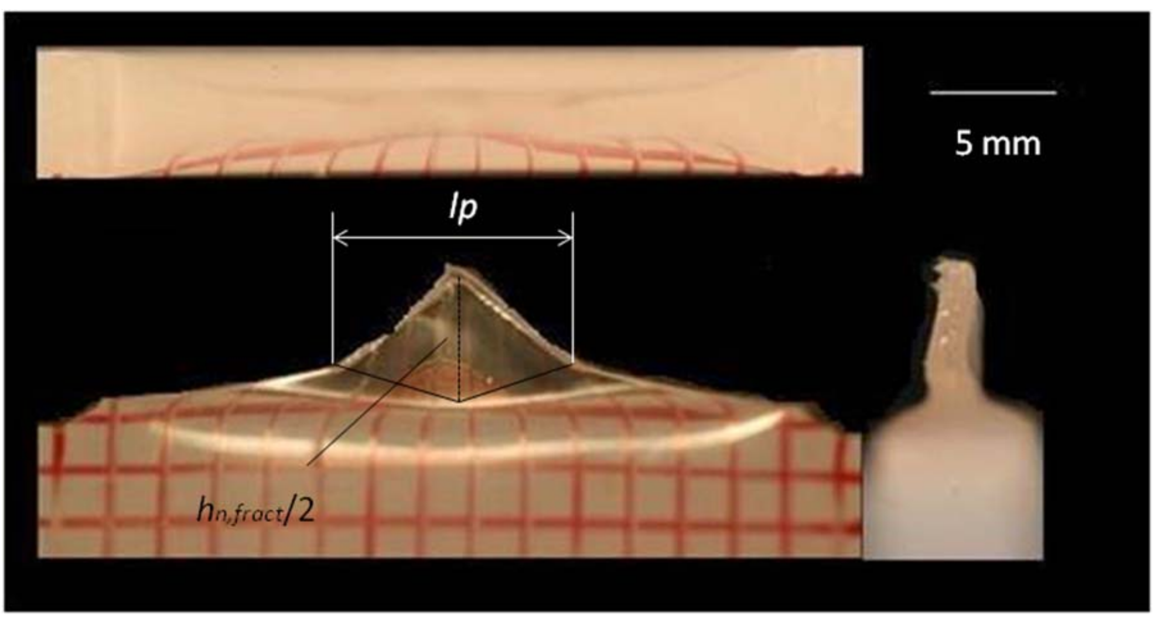

(b)

Fig.2-4 Typical experimental observations: (a) load-displacement curve from the DENT tests (taken from a specimen with l_0=34 mm), and (b) top, front, and side views of a DENT specimen (l_0=32 mm) after the test.

2.3.1 Calculation for the shifting factor

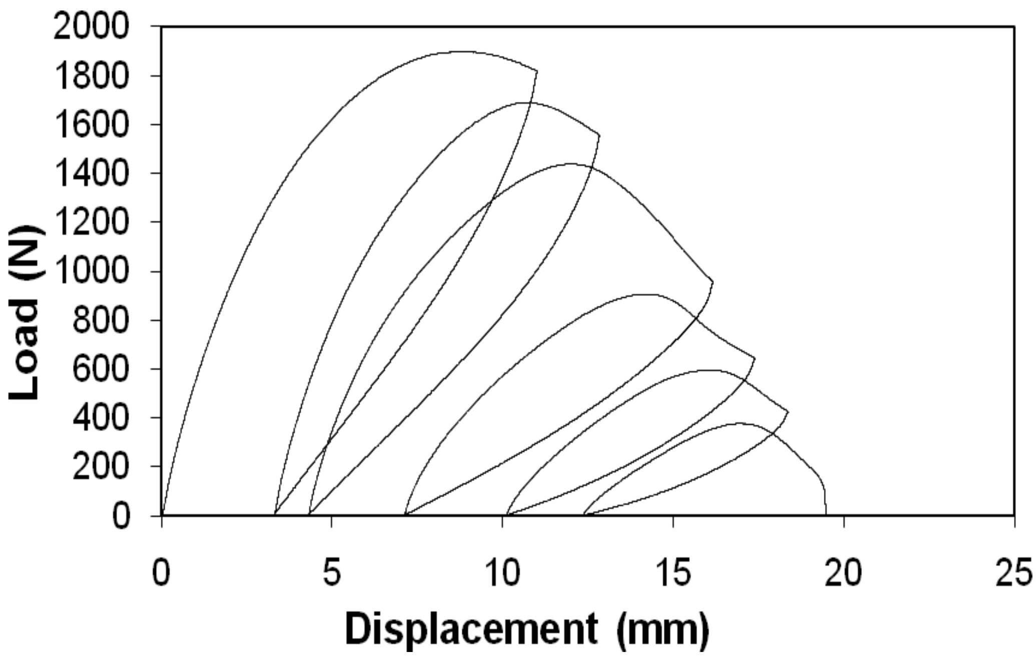

Fig.2-5 An example of the loading-unloading curves obtained from the study (in this case l_0=30 mm)

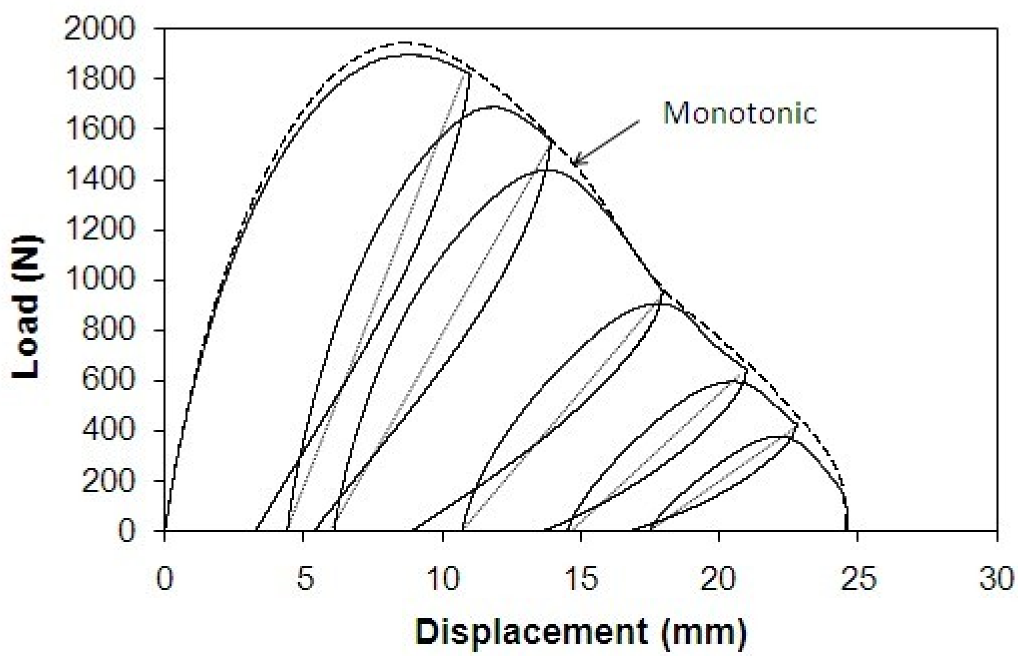

Fig.2-6 An example of the modified curve from a loading-unloading test conducted in the study (l_0=30 mm), to determine variation of stiffness during the DENT test.

Besides the specimens used for the DENT test of monotonic loading, additional eight specimens were used in loading-unloading tests to determine the variation of unloading stiffness with the crack growth, in which 5 intermittent unloading-reloading cycles were introduced in each test, two of which were introduced at the neck initiation stage (i.e. with neck growth in the ligament length direction) and the other three at the neck propagation stage (i.e. with neck growth in the loading direction), as shown in Fig. 2-5. Note that, at the end of each unloading-reloading cycle, the loading level could not return to the same level as that before the unloading-reloading cycle, i.e. a gap existing for the loading level before and after the unloading-reloading cycle. This may be because of the change of molecular structure due to the necking process. However, further investigation is required to elucidate causes for the behavior.

To eliminate the gap between the loading levels before and after each of the unloading-reloading cycle, a method was developed, details of which are given below. Fig. 2-6 presents the final curve after the modification from Fig. 2-5 using this method.

Each of the original curves from the unloading-reloading test could be divided into five parts according to the five unloading-reloading cycles. Then, each of the five parts was shifted to the position expected from the curve of monotonic loading (the dash curve in Fig. 2-6). For each part, two points were selected in the relatively straight section that is nearly parallel to the corresponding section in the curve of monotonic loading, one being close to the end of the reloading section and the other to the beginning of the unloading section. Only data from the neck propagation stage (totally six points for each curve) were used to determine the distance required for the shifting from the original position (i.e. from positions in Fig. 2-5) to the adjusted position (in Fig. 2-6), as only fracture at this stage represents the plane-stress condition.

After the shifting, the unloading stiffness was determined based on the slope of the dashed lines shown in Fig. 2-6. Note that same as that adopted in the previous study [19], the hysteresis loop was ignored for determining the stiffness.

2.3.2 Crack growth speed

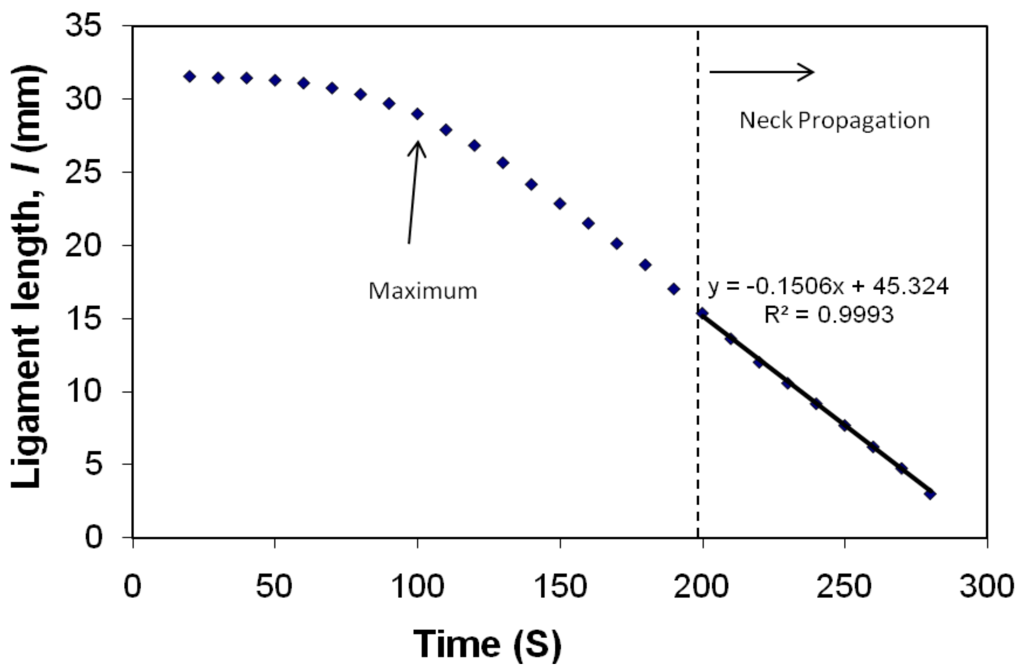

(a)

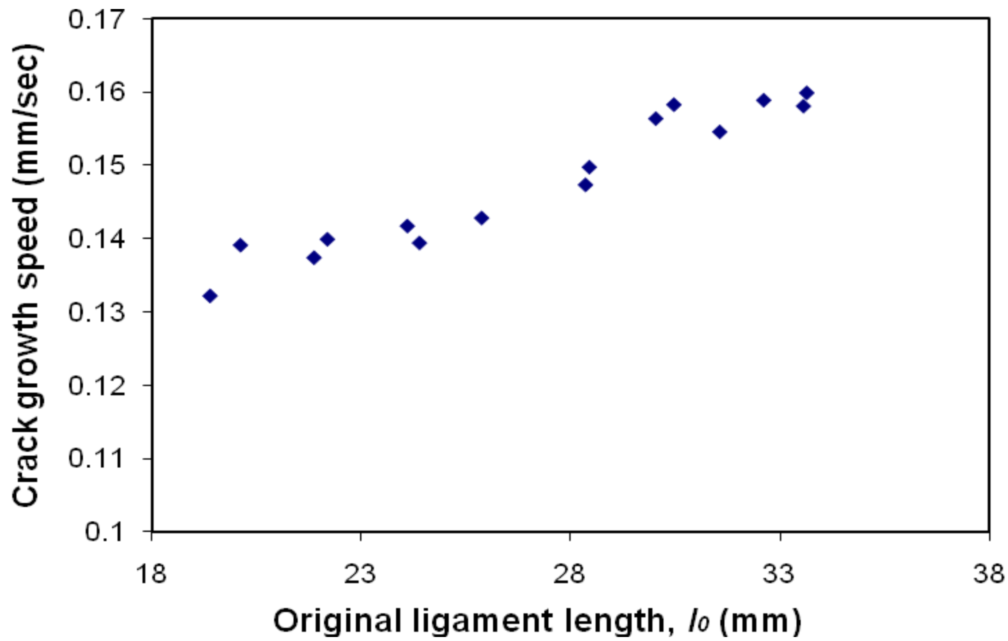

(b)

Fig.2-7 Measurement of crack growth during the DENT test: (a) variation of ligament length as a function of time, with time recorded from the beginning of the test, and (b) crack growth speed at the neck propagation stage as a function of the original ligament length (l_0).

The crack growth speed in LDPE specimens was found to be constant during the neck propagation stage, except at the very end where a significant decrease of ligament length occurs suddenly. Fig. 2-7a gives an example, which indicates that the rate of ligament length reduction is low before the maximum loading point, but then increases to become nearly constant at both neck initiation and neck propagation stages. Note that the rate of ligament length decrease for LDPE does not show any noticeable change during the transition between the two stages, which is different from that shown in HDPE [19].

Fig. 2-7b shows the crack growth speed at neck propagation stage, as a function of the original ligament length. The figure suggests that the crack growth speed increases around 20% with the increase of the original ligament length, from 20 to

34 mm. As a result, the change of the crack growth speed over the range of original ligament length l_0 used in the study is not negligible. In view of this, the crack growth speed value (V_c) was determined for each specimen, as listed in Table 2-1:

Table 2-1 The values of crack growth speed for all specimens.

l_0 (mm)	Vc (mm/s)
33.6	0.160
33.6	0.158
32.6	0.159
31.6	0.151
30.5	0.158
30.0	0.156
28.4	0.147
25.9	0.141
25.9	0.143
24.4	0.139
24.1	0.142
22.2	0.140
21.9	0.137
20.1	0.139
19.4	0.132

2.3.3 Load-displacement curve

In the previous study on HDPE [19], all of the load-displacement curves were converted to a master curve by choosing a proper shifting factor. However, curves from LDPE used in this study could not be converted in the same way. Therefore, the calculation was based on individual load-displacement curve. Also, following the method discussed in reference [19], each curve was normalized by the maximum load (F_{max}) and the displacement at fracture (δ_{fract}), as given in Fig. 2-8.

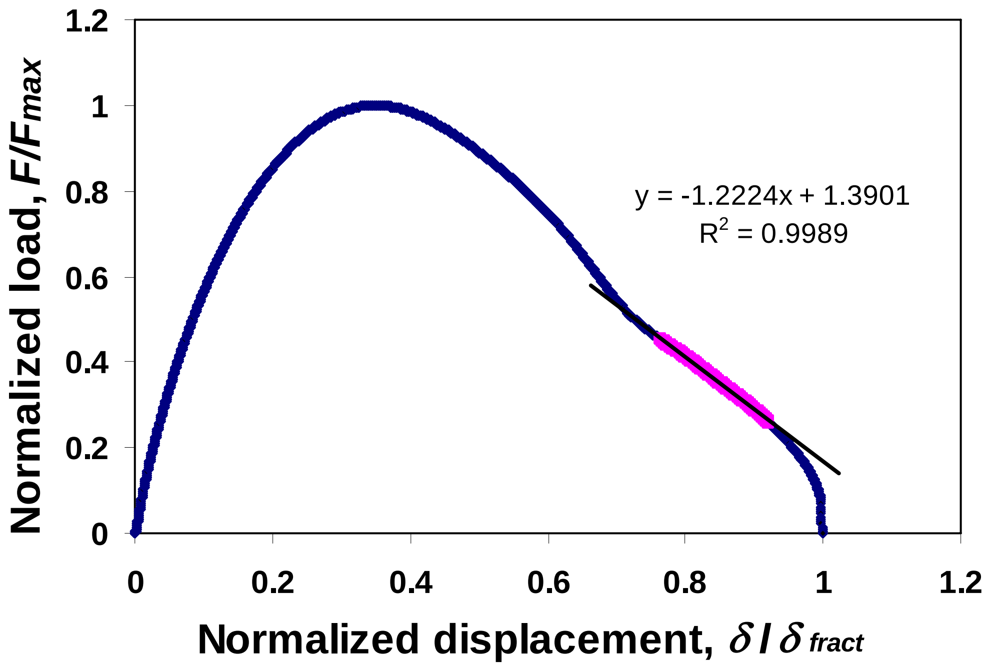

Fig.2-8 An example of the normalized load-displacement curve, from a specimen with l_0 = 32 mm.

For LDPE used in this study, the function that describes all load-displacement curves at the neck propagation stage is:

$$\frac{F}{F_{\max}} = -p\frac{\delta}{\delta_{fract}} + q \tag{2-6}$$

where F and δ are load and displacement, respectively, and p and q are constant determined from the governing equation for the neck propagation stage of the normalized curve. Values of constants p and q for each specimen are listed in Table 2-2.

Table 2-2 The values of constants p and q for all the specimens.

l_0 (mm)	p	q
32.6	1.2592	1.4087
31.6	1.2224	1.3901
33.6	1.2400	1.4038
33.6	1.2503	1.4206
30.0	1.2770	1.4355
30.5	1.2417	1.4027
28.4	1.2168	1.3676
25.9	1.2711	1.4449
25.9	1.1401	1.2963
24.1	1.1719	1.3295
24.4	1.0884	1.2546
22.2	1.1468	1.2983
21.9	1.1054	1.2633
19.4	1.0984	1.2537
20.1	1.1196	1.2743

2.3.4 Unloading stiffness

As discussed in section 2.2.2, seven specimens, with the original ligament length in the range from 20 to 34 mm, were tested in this study to determine the unloading stiffness (m) at the neck propagation stage. The trend was found to follow a linear relationship with the normalized displacement. As shown in Fig. 2-9, m value decreases with the increase of the normalized displacement (δ/δ_{fract}), and their relationship can be approximated as:

$$m = -260.02\frac{\delta}{\delta_{fract}} + 318.4 \tag{2-7}$$

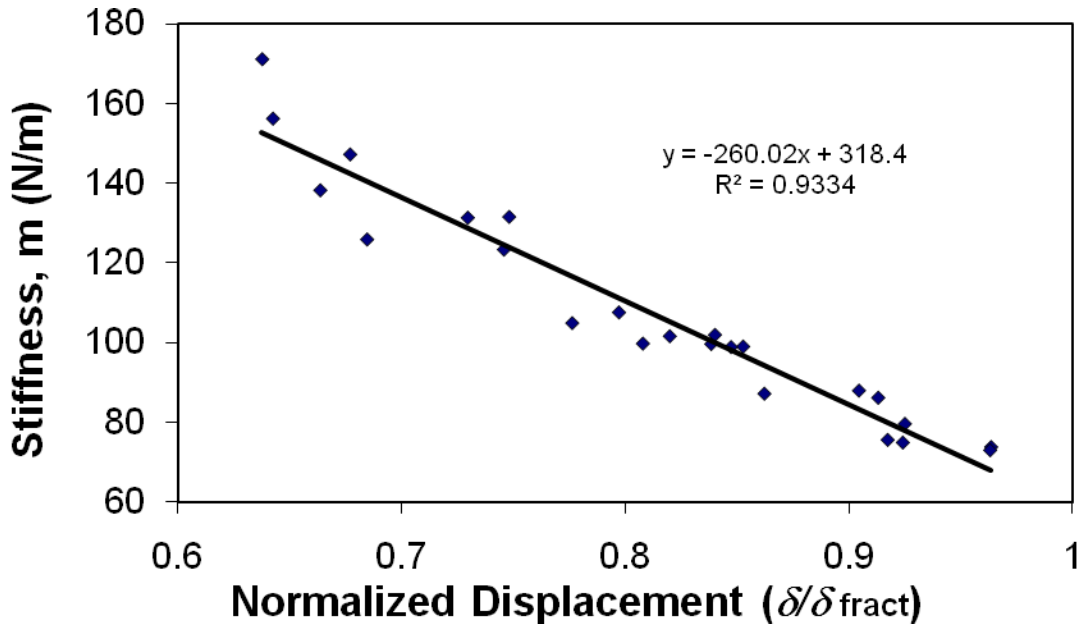

Fig.2-9 Variation of stiffness in the neck propagation stage, plotted as a function of the normalized displacement (δ/δ_{fract}).

2.4 The new approach and formulation of energy balance equation

The new approach adopted in this study is based on the energy balance concept, to deduce equations that include all mechanisms involved in the fracture process. Same as before, the viscoelastic behavior of LDPE was ignored in order to simplify the calculation for the unloading stiffness, so that the unloading stiffness could be determined based on the slope of dashed lines shown in Fig. 2-5. As discussed in the previous section, plane-stress fracture occurs at the neck propagation stage of LDPE, therefore, only mechanisms involved at this stage were considered to establish the energy formulation.

Fig. 2-10a shows the front view of a DENT specimen at the neck propagation stage, which indicates a significant stretch of the mesh in the loading direction.

The area (named as active deformation zone) that is enclosed by the white dashed lines in the figure is where the deformation was still actively generated by the loading.

Fig. 2-10b presents all mechanisms involved in the active deformation zone at the neck propagation stage. Different from the original EWF method in which only mechanisms (i), and (ii), for the fracture surface formation and neck growth, respectively, are considered, the new approach considers an additional mechanism in the fracture process, i.e. (iii) shear plastic deformation that results in the triangular contour, as depicted in Fig. 2-10b. The corresponding energy densities for mechanisms (i) (ii) and (iii) are w_e, $w_{p,n}$ and $w_{p,s}$, respectively, which are corresponding to formation of unit fracture surface, development of unit neck volume and generation of unit shear plastic deformation volume. Note that $w_{p,n}$ has different definition from w_p in the original EWF method. That is, $w_{p,n}$ is the specific energy consumed by necking, while w_p represents energy consumed by all kinds of plastic deformation.

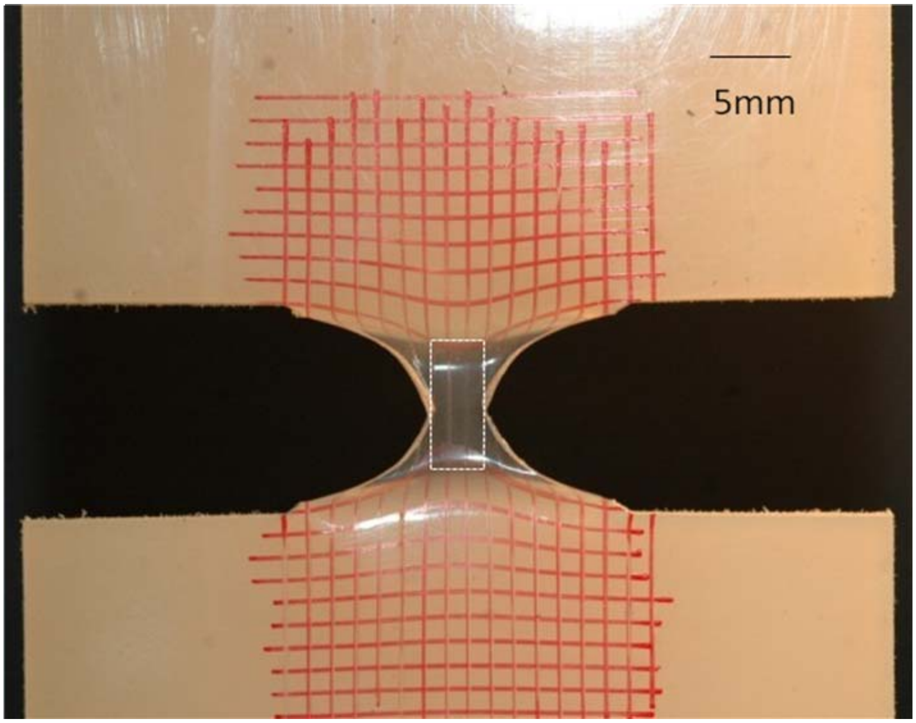

(a)

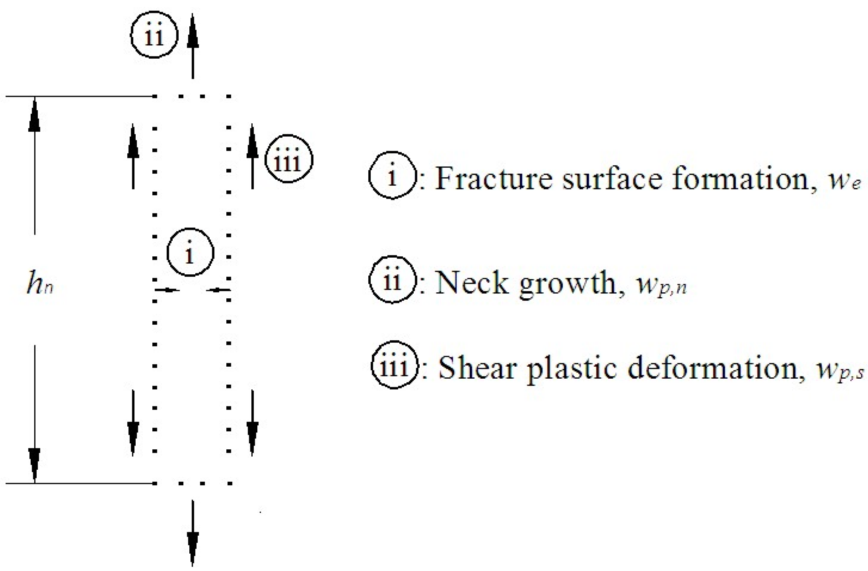

(b)

Fig.2-10 Depiction of deformation behaviour in the DENT test: a snap shot during the neck propagation stage.

Since the crack growth speed remains constant at the neck propagation stage, the neck growth speed and the shear plastic deformation rate should be constant during this stage, to form the quadrilateral-shaped active deformation zone, as shown in Fig. 2-10b. For the same reason, the height h_n in Fig. 2-10b can be expressed as a linear function of time as:

$$h_n = h_0 + \beta_h V_\delta t \tag{2-8}$$

where h_0 is the original height of the active deformation zone and β_h a constant, both of which need to be determined from experiments. t is the time measured from the beginning of neck propagation stage, i.e. at the right dashed line in Fig. 2-10a, and V_δ the cross-head speed for the DENT test.

Based on the energy balance concept, all of the energy consumed for the three mechanisms, plus the change of strain energy, should be equal to the external work input. That is:

$$w_e dA + w_{p,n} dV_n + w_{p,s} dV_s = -dU + F d\delta \tag{2-9}$$

where A is the fracture surface area, V_n the volume of the necking zone, V_s the volume of shear plastic deformation zone, U the strain energy, F the load and δ the corresponding displacement. In Equation (2-9), dA, dV_n and dV_s can be expressed in terms of the crack growth speed (V_c) at the neck propagation stage and the cross-head speed (V_δ) as:

$$dA = 2 t_n V_c dt \tag{2-10a}$$

$$dV_n = t_n l \beta_h V_\delta dt \tag{2-10b}$$

$$dV_s = 2t_n V_c h_n dt \tag{2-10c}$$

where t_n is the ligament thickness of the fully-necked section and l the remaining ligament length at time t.

By assuming a linear relationship between load and displacement during the unloading, the strain energy stored in the specimen can be expressed as a function of load F and stiffness m as:

$$U = \frac{F^2}{2m} \tag{2-11}$$

Therefore,

$$dU = \frac{F}{m}dF - \frac{F^2}{2m^2}dm \tag{2-12}$$

After substituting Equations (2-10) and (2-12) to (2-9), the expression below can be obtained:

$$(2t_n V_c) w_e dt + (t_n l \beta_h V_\delta) w_{p,n} dt + (2t_n V_c h_n) w_{p,s} dt = -\frac{F}{m}dF + \frac{F^2}{2m^2}dm + Fd\delta \tag{2-13}$$

Since the crack growth speed V_c is considered constant at the neck propagation stage, time t can be expressed as a function of ligament length l as:

$$t = \frac{(l_p - l)}{2V_c} \tag{2-14}$$

Thus,

$$dt = -\frac{dl}{2V_c} \tag{2-15}$$

Similarly, displacement δ can be expressed as a function of l:

$$\delta = \delta_c + V_\delta \frac{(l_p - l)}{2V_c} \tag{2-16}$$

Thus,

$$d\delta = -\frac{V_s}{2V_c} dl \tag{2-17}$$

where δ_c is the displacement at the commencement of the neck propagation stage.

By substituting dt and $d\delta$ to Equations (2-15) and (2-17), after canceling the common term dl, the following expression can be obtained.

$$-t_n w_e - \frac{1}{2V_c}[w_{p,n} t_n l \beta_h V_\delta + 2w_{p,s} t_n h_n V_c] = -\frac{F}{m} \times \frac{dF}{dl} + \frac{F^2}{2m^2} \times \frac{dm}{dl} - \frac{FV_\delta}{2V_c} \tag{2-18}$$

Then, by replacing F, m and h_n in Equation (2-18), the following expression can be generated:

$$
\begin{aligned}
& -t_n V_c w_e - \frac{1}{2}(w_{p,n} t_n l \beta_h V_\delta + 2 w_{p,s} t_n (h_0 + \beta_h V_\delta \frac{l_p - l}{2V_c}) V_c) \\
& = -x F_{\max} \frac{V_\delta F_{\max}(-x \frac{V_\delta l_p + 2V_c \delta_c}{V_c \delta_f} + y + x \frac{V_\delta}{V_c \delta_f} l)}{\delta_f (z \frac{V_\delta l_p + 2V_c \delta_c}{V_c \delta_f} + w + z \frac{V_\delta}{V_c \delta_f} l)} \\
& + z \frac{V_\delta F_{\max}^2 (-x \frac{V_\delta l_p + 2V_c \delta_c}{V_c \delta_f} + y + x \frac{V_\delta}{V_c \delta_f} l)^2}{2\delta_f (z \frac{V_\delta l_p + 2V_c \delta_c}{V_c \delta_f} + w + z \frac{V_\delta}{V_c \delta_f} l)^2} \\
& + F_{\max}(-x \frac{V_\delta l_p + 2V_c \delta_c}{V_c \delta_f} + y + x \frac{V_\delta}{V_c \delta_f} l) \times (-\frac{V_\delta}{2})
\end{aligned}
\tag{2-19}
$$

After rearrangement by putting together all terms with the same order of l, we have:

$$
\begin{aligned}
& (a^2 g w_e + \frac{1}{2} a^2 c) + [2abgw_e + \frac{1}{2}(a^2 d + 2abc)]l + [b^2 g w_e + \frac{1}{2}(2abd + b^2 c)]l^2 + \frac{d}{2} l^3 \\
& = (aeh - e^2 i + a^2 ej) + [(af + be)h - 2ef + (a^2 f + 2abe) j]l + [bfh - f^2 i + (2abf + b^2 e) j]l^2 + fjl^3
\end{aligned}
\tag{2-20}
$$

where

$$a = -\frac{2il_p}{F_{\max}^2 V_c} + m_c \tag{2-21a}$$

$$b = \frac{2i}{F_{\max}^2 V_c} \tag{2-21b}$$

$$c = t_n w_{p,s} (2h_0 V_c + \beta_h V_\delta l_p) \tag{2-21c}$$

$$d = (w_{p,n} - w_{p,s}) t_n \beta_h V_\delta \tag{2-21d}$$

$$e = -\frac{hl_p}{F_{\max}^2 V_c} + \frac{F_c}{F_{\max}} \tag{2-21e}$$

$$f = \frac{h}{F_{\max}^2 V_c} \tag{2-21f}$$

$$g = t_n V_c \tag{2-21g}$$

$$h = x\frac{F_{\max}^2 V_\delta}{\delta_{fract}} \tag{2-21h}$$

$$i = \frac{z}{2x} h \tag{2-21i}$$

$$j = \frac{F_{\max} V_\delta}{2} \tag{2-21j}$$

where $x = p/2$, $y = q$ (p and q are constants in Equation (2-6)), w = 318.4 and z = 260.02/2, 318.4 and 260.2 are the two constants in Equation (2-7) and m_c and F_c represent stiffness and load at the beginning of neck propagation stage, respectively. Note that in Equation (2-21) only c and d contain unknown values of h_0 and β_h, which will be discussed later.

In Equation (2-20), l is a free variable with values changing from l_p to zero at the neck propagation stage. Therefore, the equation holds only if the following four expressions (for the same order of l) are satisfied:

from l^0 terms

$$a^2 g w_e + \frac{1}{2} a^2 c = aeh - e^2 i + a^2 ej \tag{2-22a}$$

from l^1 terms

$$2abgw_e + \frac{1}{2}(a^2 d + 2abc) = (af + be)h - 2efi + (a^2 f + 2abe)j \tag{2-22b}$$

from l^2 terms

$$b^2 g w_e + \frac{1}{2}(2abd + b^2 c) = bfh - f^2 i + (2abf + b^2 e)j \tag{2-22c}$$

from l^3 terms

$$\frac{d}{2} = fj \tag{2-22d}$$

Through substitution of Equation (2-21d) to Equations (2-21b) and (2-21c), we have:

$$2abgw_e + abc = (af + be)h - 2efi + 2abej \tag{2-23a}$$

$$b^2 g w_e + \frac{b^2 c}{2} = bfh - f^2 i + b^2 ej \tag{2-23b}$$

After normalization to make the coefficient for w_e be equal to 1, Equations (2-22a), (2-23a) and (2-23b) can be rewritten as:

$$w_e + \frac{1}{2g} c = \frac{eh}{ag} - \frac{e^2 i}{a^2 g} + \frac{ej}{g} \tag{2-24a}$$

$$w_e + \frac{1}{2g}c = (\frac{f}{2bg} + \frac{e}{2ag})h - \frac{efi}{abg} + \frac{ej}{g} \tag{2-24b}$$

$$w_e + \frac{1}{2g}c = \frac{fh}{bg} - \frac{f^2 i}{b^2 g} + \frac{ej}{g} \tag{2-24c}$$

Equations (2-24b) and (2-24c) are found to be identical, which can be rewritten as:

$$w_e + \frac{1}{2g}c = \frac{V_\delta(\delta_{fract}F_c \frac{z}{x}V_c + F_{\max}x(F_{\max}V_c - l_p \frac{z}{x}V_\delta))}{2\delta_{fract}\frac{z}{x}t_n V_c^2} \tag{2-25}$$

Table 2-3 List of values for the right-hand side (RHS) of Equations (2-24a) and (2-25), β_h and h_0 for all specimens.

l_0(mm)	RHS of Eq. (2-24a)	RHS of Eqn. (2-25)	β_h	h_0 (mm)
32.6	183	260	1.22	5.54
31.6	181	256	1.25	4.34
33.6	182	267	1.25	5.25
33.6	179	256	1.25	4.85
30.0	164	243	1.24	4.67
30.5	171	245	1.25	4.76
28.4	164	242	1.24	4.32
25.9	165	218	1.24	4.44
25.9	160	220	1.23	4.19
24.1	149	201	1.25	3.81
24.4	161	205	1.26	4.07
22.2	145	192	1.24	3.24
21.9	145	187	1.23	3.35
19.4	130	166	1.24	3.46
20.1	135	174	1.25	3.64

As shown in Table 2-3, there is around 25% difference between values for the terms on the right-hand side of Equations (2-24a) and (2-25). It is believed that this is caused by inconsistency between monotonic loading curve and the loading-unloading curve in section 2.3.1. Also, it was found that value of Equation (2-24a) is dependent on values of both constants in Equation (2-7) (i.e. -260.02 and 318.4) while Equation (2-25) does not depend on the constant 318.4 at all. Table 2-4 shows that, by changing the value of q in Equation (2-6), $w_{p,s}$ and w_e values are not changed, thus not truly representing the expected change in energy balance formulation. Therefore, Equation (2-24a) should be used, instead of Equation (2-25). Note that in Table 2-4, when q is smaller than 200, the fitting curve of Equation (2-24a) shows a very poor linear relationship, which results in the dramatic fluctuation at the first lines of the table.

Table 2-4 List of values of specific works of fracture determined using Equations (2-24a) and (2-25), based on variable q values.

	Equation (2-24a)		Equation (2-25)	
q	$w_{p,s}$ (KJ/m^3)	w_e (KJ/m^2)	$w_{p,s}$ (KJ/m^3)	w_e (KJ/m^2)
0	-9000	21.5	22000	-18.2
50	-12000	-76.9	22000	-18.2
100	3470000	-5360	22000	-18.2
150	10000	79.2	22000	-18.2
200	18000	2.6	22000	-18.2
250	14000	25.1	22000	-18.2
300	12000	35.9	22000	-18.2
318.4	11400	38.2	22000	-18.2
350	10600	41.1	22000	-18.2

By substituting the parameter c in Equation (2-21c) to Equation (2-24a), an explicit expression for the relationship between w_e and $w_{p,s}$ can be found:

$$w_e + \frac{t_n(2h_0V_c + \beta_h V_\delta l_p)}{2g} w_{p,s} = \frac{eh}{ag} - \frac{e^2 i}{a^2 g} + \frac{ej}{g} \quad (2\text{-}26)$$

Also, Equation (2-22d) gives an expression for the relationship between $w_{p,n}$ and $w_{p,s}$:

$$(w_{p,n} - w_{p,s}) t_n \beta_h = \frac{dF}{dl} \quad (2\text{-}27)$$

According to Equation (2-26), values of w_e and $w_{p,s}$ can be determined by linear regression for the plot of $(\frac{t_n(2h_0V_c + \beta_h V_\delta l_p)}{2g})$ versus $(\frac{eh}{ag} - \frac{e^2 i}{a^2 g} + \frac{ej}{g})$. That is, w_e is the intercept at the vertical coordinate and $w_{p,s}$ is the slope of the plot. As a result, the corresponding $w_{p,n}$ value can be determined from Equation (2-26).

After the above analysis, the remaining barrier is to determine the values of h_0 and β_h in Equation (2-27). Based on the principle of volume continuity and incompressibility at the neck growth front, β_h value was determined following the approach given in Ref. [21]:

$$\beta_h = \frac{t_0}{t_0 - t_n \frac{b_n}{b_0}} \quad (2\text{-}28)$$

where b_0 and b_n are the original mesh width in the central ligament region and the corresponding dimension after the neck is fully developed. Once the β_h value was determined, the h_0 value can then be calculated using Equation (2-8). That is, the expression is:

$$h_0 = h_{n,fract} - \beta_h V_\delta \frac{l_p}{2V_c} \tag{2-29}$$

Values of β_h and h_0 for all specimens used in this study are listed in Table 2-3, which suggest that with the decrease of the original ligament length l_0, h_0 decreases significantly while β_h does not change much.

2.5 Discussion

In this section, w_e values determined from different methods, i.e. the new mechanistic approach, the original EWF method and energy partition method, will be compared first. It will be shown that those approaches yield different w_e values, among which the latter two methods agree with each other well. To verify validity of those methods for LDPE, $w_{p,n}$ from simple tensile test was used for the evaluation.

2.5.1 Comparison of w_e values

Fig. 2-11 presents the plot of $(\frac{t_n(2h_0V_c + \beta_h V_\delta l_p)}{2g})$ versus $(\frac{eh}{ag} - \frac{e^2 i}{a^2 g} + \frac{ej}{g})$ using values of h_0 and β_h in Table 2-3 from which values for w_e and $w_{p,s}$ were determined and listed in Table 2-4. Value for $w_{p,n}$ was then determined using Equation (2-27).

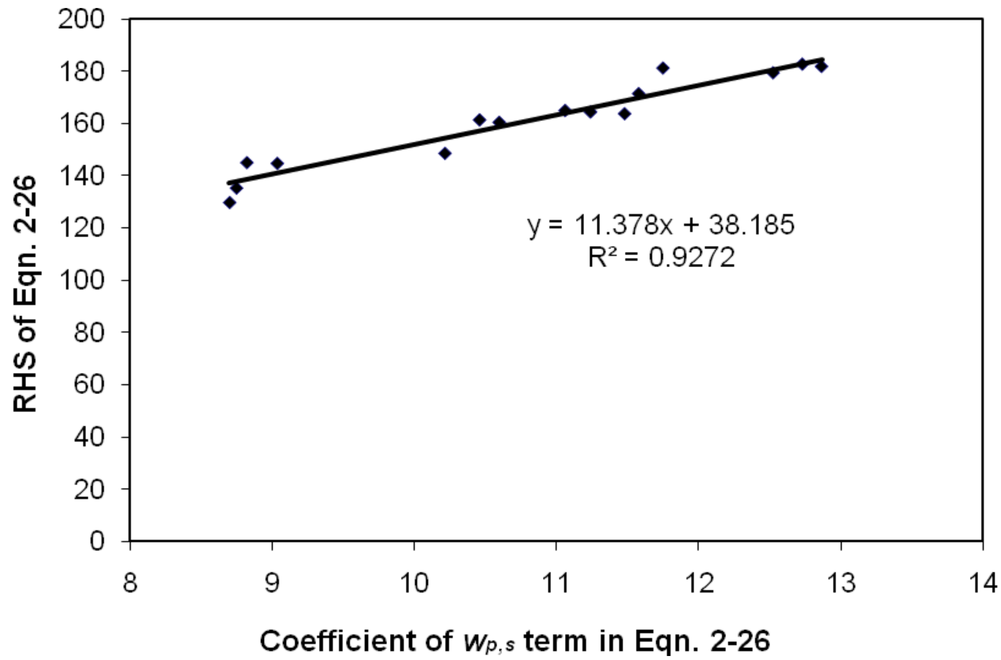

Fig.2-11 Regression plot of right-hand side of Eqn. 2-26 versus coefficient of the $w_{p,s}$ term in the same equation.

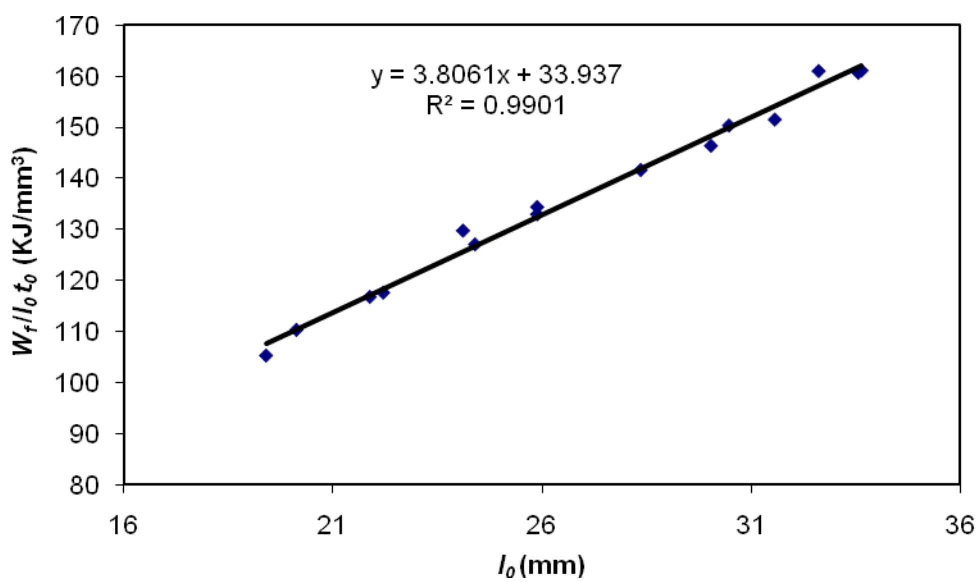

(a)

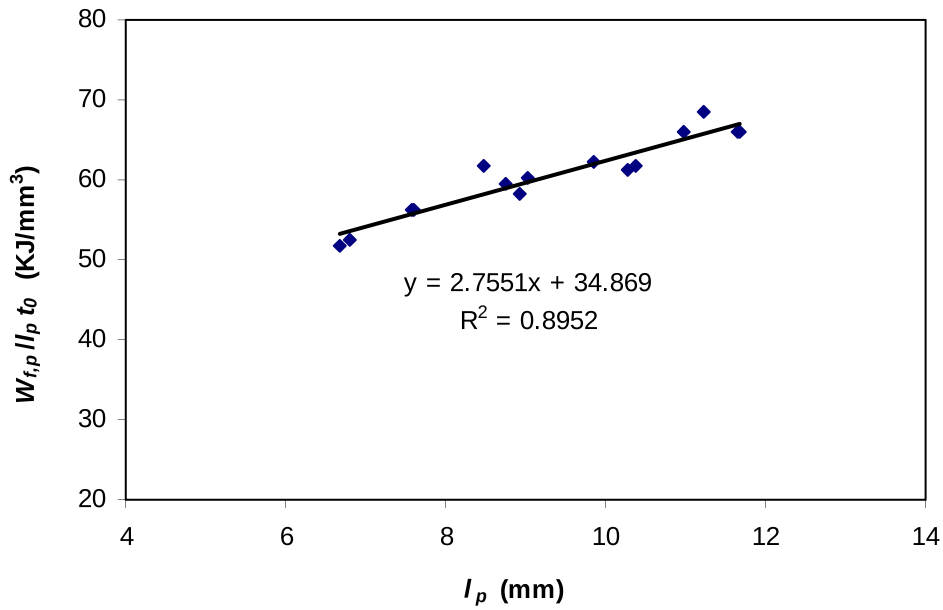

(b)

Fig.2-12 Regression plots based on (a) specific total work of fracture, $W_f/(l_0\,t_0)$, and (b) energy partition, $W_{f,p}/(l_p\,t_0)$.

Fig. 2-12a is the linear regression of the normalized total work fracture, $W_f/(\,l_0\,t_0)$ and Fig. 2-12b is the normalized work input at the neck propagation stage, $W_{f,p}/(\,l_p\,t_0)$. Results from Fig. 2-12 are based on the same tests as those for Fig. 2-11, from which w_e values are determined to be 33.9 (Fig. 2-11) and 34.9 KJ/m^3 (Fig. 2-12), respectively. All values are listed in Table 2-5. Although those w_e values are close to each other, the value from the new approach is slightly different from the other two. Nevertheless, difference among those values does not justify their validity, since no other method is available to quantify the fracture resistance accompanied by such large deformation. Instead, an alternative method is used for the evaluation, by comparing $w_{p,n}$ value from the new approach with that from the simple tensile test. Note that data in Fig. 2-12a show better linear correlation than those in the other figures, possibly because the original EWF method does not require quantification of any additional parameters through measurement, such as h_0 and β_h in the new approach, and l_p in the energy partition approach. However, good linear correlation does not serve as an indication for the correctness of the fracture toughness value.

Table 2-5 Results from the new approach, and those from EWF approach based on either total fracture or energy partition.

	New approach	EWF (total work of fracture)	EWF (energy partition)
w_e (KJ/m^2)	38.2	33.9	34.9
$w_{p,n}$ (KJ/m^3)	35,200	-	-
$w_{p,s}$ (KJ/m^3)	11,400	-	-
βw_p (KJ/m^3)	-	3.8	2.8

2.5.2 Comparison with results from tensile test

Dog-bone specimens (type I of ASTM Standard D638) were used in this study to determine the necking energy density from simple tensile test. The tests followed a cross-head speed of 3 mm/min.

Fig. 2-13 is a typical load-displacement curve from the simple tensile test. Since LDPE necks relatively uniformly along the loading direction, neck front cannot be clearly detected during the test. In view of this, the energy density for necking was determined by dividing the total energy for neck formation by the total necking volume, as shown below:

$$w_n = \frac{Eu}{A_0 l_1} \tag{2-30}$$

where w_n is the necking energy density, Eu the total energy consumed for plastic deformation during the neck formation, A_0 the original cross-sectional area, and l_1 the original gauge length that corresponds to the necking part of the specimen.

Due to relatively uniform neck formation in the gauge section, based on the principle of volume conservation, cross-sectional areas before and after the necking and crosshead displacement should satisfy the following expression:

$$(A_0 - A_n)l_1 = A_n(\delta_2 - \delta_1) \tag{2-31}$$

where A_0 and A_n are the cross-sectional areas before and after the neck is fully developed, respectively, δ_1, as presented in Fig. 2-13, is the displacement at the beginning of the necking process, and δ_2 the displacement at which the cross-sectional area of the specimen does not shrink anymore, which also corresponds to the end of the necking process. Note that, the choice of δ_1, instead of zero, was to exclude the elastic energy.

The specific necking energy density determined from the simple tensile test was found to be 30,400 KJ/m^3 which is about 14% lower than the $w_{p,n}$ value from DENT test determined using the new mechanistic approach. Since it is not possible to determine w_p value due to the unknown β value and that βw_p from the total work of fracture is just a mean value of energy density for plastic deformation, due to the non-uniform necking process in the DENT test, it is not possible to evaluate correctness of βw_p values. Also, there has not been any attempt to justify βw_p value without identifying the shape of the plastic deformation zone. The closeness of the two w_e values in Table 2-5 may be because the load-displacement curve of LDPE is smooth. As a result, the energy consumed is proportional to the displacement.

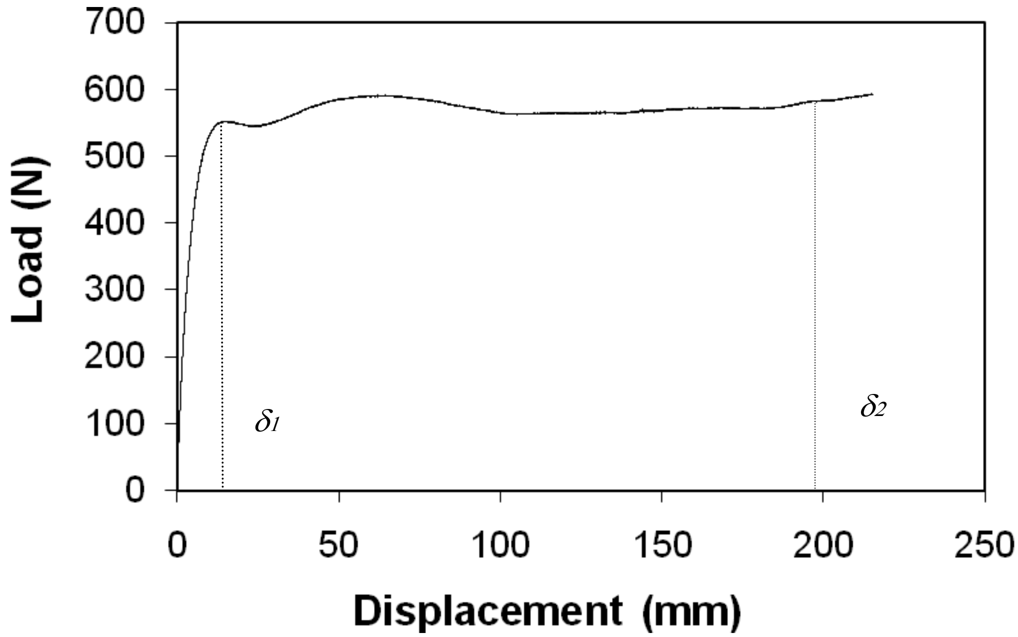

Fig.2-12 Typical load-displacement curve from the simple tensile test.

2.6 Conclusions

The fracture behavior of LDPE in DENT test can be divided into neck initiation and neck propagation stages. It was found by observation that only at the second stage, LDPE shows plane-stress fracture behavior. During the neck propagation stage, three mechanisms, i.e. fracture surface formation, shear plastic deformation and neck growth, were observed. Using linear regression, specific energy densities for the three mechanisms were determined using a new mechanistic approach based on the principle of energy conservation.

For all three parameters determined from the new approach, only the w_e value can be compared directly with those based on the EWF concept. Difference of the w_e values for the LDPE used in the study was found to be small. To justify validity of those values, specific energy for necking in a simple tensile test was determined. It was found that the necking energy density from the new approach and that from the simple tensile test are similar (only around 14% in difference). However, because of the smaller fracture strain for the simple tensile test (1.44 compared to 1.64 in the DENT test, or around 12% smaller), it is reasonable that the specific necking energy density form the simple tensile test is slightly smaller than $w_{p,n}$ from the DENT test. Since there is no method to determine whether the plastic energy density βw_p is accurate, it is not certain whether the corresponding w_e value from the original EWF method can be used to represent fracture toughness of the LDPE. On the other hand, the necking energy density from the simple tensile test provides some sort of support to the validity of the new mechanistic approach for characterizing the plane-stress fracture toughness of LDPE.

References

[1] Broberg KB. Critical review of some theories in fracture mechanics. Int J Fracture 1968; 4:11-8.

[2] Broberg KB. Crack–growth criteria and non-linear fracture mechanics. J Mech Phys Solids 1971;19:407-18.

[3] Briberg KB. On stable crack growth. J Mech Phys Solids 1975; 23: 215-37.

[4] Cotterell B, Reddel JK. The essential work of plane stress ductile fracture. J Int Fract 1977; 13: 267-277.

[5] Mai YW, Cotterell B. The essential work for tearing of ductile metals. Int J Fracture 1984; 24: 229-36.

[6] Mai Y-W, Wong S-C, Chen X-H. Application of fracture mechanics for characterization of toughness of polymer blends. In: Paul DR, Bucknall CB, editors. Polymer blends: formulations and performance, Vol 2. NewYork: Wiley; 2000. P. 17-58.

[7] Mai YW, Cotterell B. On the essential work of ductile fracture in polymers. Int J Fracture 1986; 32: 105-25.

[8] Mai YW, Powell P. Essential work of fracture and J-integral measurements for ductile polymers. J Polym Sci Part B Polum Phys 1991; 29: 785-93.

[9] Mai YW, Cotterell B, Horlyck R, Vigna G. The essential work of plane stress ductile fracture of linear polyethylenes. Polym Engng Sci 1987; 27(11):804-9

[10] Peres F, Schon C. Application of the essential work of fracture method in ranking the performance in service of high-density polyethylene resins employed in pressure pipes. J Mater Sci 2008; 43(6): 1844-50.

[11] Kwon HJ, Jar PYB. Application of essential work of fracture concept to toughness characterization of high-density polyethylene. Polym Engng Sci 2007; 47(9): 804-9.

[12] Maspoch ML, Ferrer D, Gordillo A. Effect of the specimen dimensions and the test speed on the fracture toughness of iPP by the essential work of fracture (EWF) method. J Appl Polym Sci 1999; 73(2): 177-87.

[13] Hashemi S. Determination of the fracture toughness of polyethylene terephthalate (PBT) film by the essential work method: effect of specimen size and geometry. Polym Engng Sci 2000; 40(3): 798-808.

[14] Levita G, Parisi L, Marchetti A. Effect of thickness on the specific essential work of fracture of rigid PVC. Polym Engng Sci 1996; 36(20): 2534-41.

[15] Hashemi S. Work of fracture of PBT/PC blend: effect of specimen size, geometry, and rate of testing. Polym Engng Sci 1997; 37(5): 912-21.

[16] Karger-Kocsis J. For what kind of polymer is the toughness assessment by the essential work concept straightforward? Polym Bull 1996; 37: 119-26.

[17] Vu-Khanh T. Impact fracture characterization of polymer with ductile behavior. Theor Appl Fract Mech 1994; 21: 83-90.

[18] Bernal CR, Frontini PM. Determination of fracture-toughness in rubber-modified glassy-polymers under impact conditions. Polym Eng Sci 1995; 35: 1705-12.

[19] Jar PYB, Adianto R. Determination of plane-strain fracture toughness of polyethylene copolymer based on the concept of essential work of fracture. Polym Engng Sci 2010; 50: 530-5.

[20] Williams JG, Rink M. The standardization of the EWF test. Engng Fract Mech 2007; 74(7): 1009-7.

[21] Neale KW, Tugcu P. Analysis of necking and neck propagation in polymeric materials. J Mech Phys Solids 1985; 33(4): 323-7.

Chapter 3 Evaluation of Ultra-high-Molecular-Weight Polyethylene Based on a Modified Essential Work of Fracture Method

3.1 Introduction

Broberg [1] is the first to propose the concept of essential work of fracture (EWF) method in 1968. He divided the total work of fracture into two parts: the dissipative work in outer "plastic" zone and essential work in the inner autonomous zone which is also called fracture process zone [2, 3].

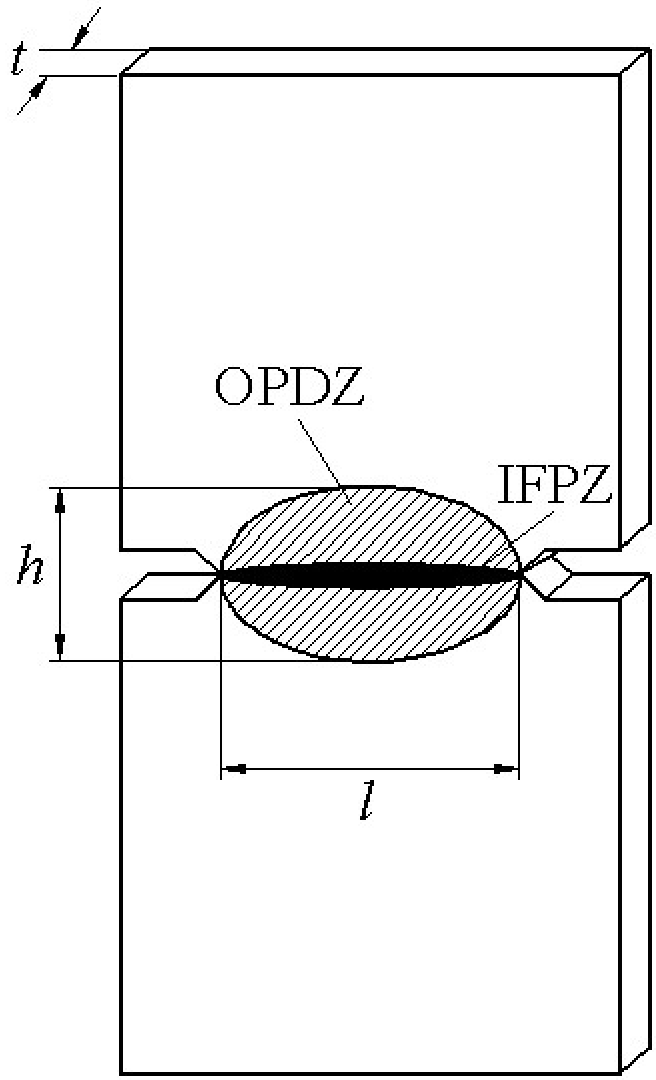

Fig.3-1 Schematic diagram showing the regions involved in the fracture (inner fracture process zone (IFPZ), and outer plastic deformation zone (OPDZ)), as proposed by Broberg [2,3].

Cotterell and Reddel [4], based on the EWF concept, were the first to develop a method for determining the property of thin, ductile metals. Mai et al. [5-7] extended the application of the EWF method to polymers. The main concept of EWF method can be given by Equation (3-1).

$$W_f = W_e + W_p \tag{3-1}$$

where W_f is the total work of fracture, W_e the essential work of fracture in the inner fracture process zone (IFPZ) and W_p the non-essential (plastic) work of fracture in the outer plastic deformation zone (OPDZ), as illustrated in Fig. 3-1.

W_e is proportional to the ligament length l and thickness t. And, OPDZ has an elliptical geometry, characterized by l, t and h, β a shape factor representing the relationship between h and l, as shown in Fig.3-1. Therefore, Equation (3-1) can be rewritten to become Equations (3-2) and (3-3):

$$W_f = w_f\, lt = w_e\, lt + \beta w_p l^2 t \tag{3-2}$$

where w_e is specific essential work of fracture, w_p specific plastic work of fracture, After normalized by lt on both sides of Equation (3-2), the following equation can be found:

$$w_f = w_e + \beta w_p l \tag{3-3}$$

Based on Equation (3-3), w_e can be determined by plotting w_f as a function of l in which βw_p is the slope of the plot. This method has been widely used to determine w_e which is the intercept on the vertical axis [5, 6, 7-15], as shown in Fig.3-2.

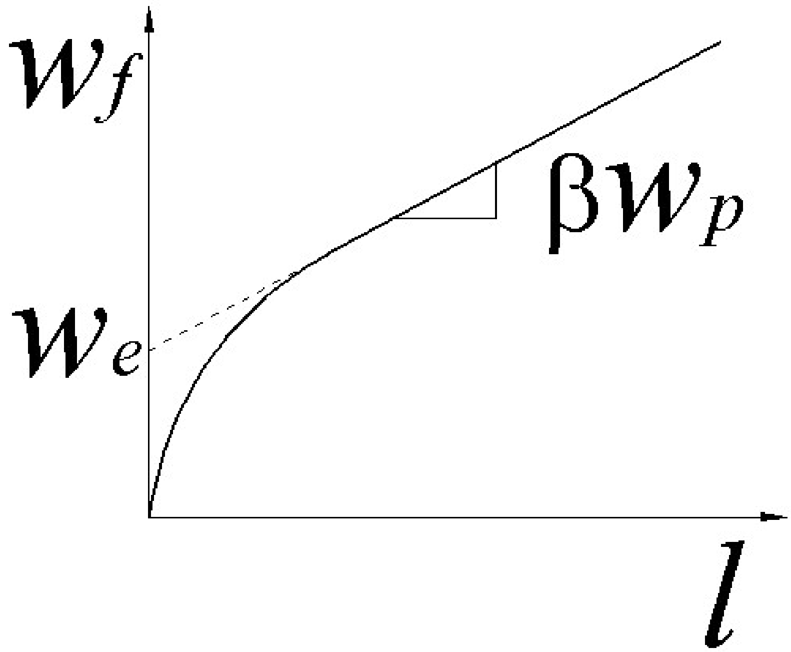

Fig.3-2 Plot of specific total work of fracture, W_f versus ligament length l.

To apply the EWF method to toughness characterization, ligament length of the specimens used for testing should meet the following condition, in order to ensure that the whole ligament yields completely before crack initiation, and that the yielding is confined to the ligament region only [4, 7].

$$(3\text{-}5)t_0 \leqslant l \leqslant min(B/3 \text{ or } 2R_p) \tag{3-4}$$

where B is width of the specimen, and R_p size of the OPDZ. R_p can be estimated using Young's modulus E and yield stress σ_y as:

$$2R_p = \frac{1}{\pi}\left(\frac{Ew_e}{\sigma_y^2}\right) \tag{3-5}$$

The value for the lower bound of Equation (3-4) is to make sure that the specimen fractures in a plane-stress condition. If l is smaller than the lower bound, the deformation state will likely fall into transition from plane-stress to plane-strain [7] which will result in the nonlinear relationship between w_f and l.

For UHMWPE, it was found that the mechanisms of necking and shear plastic deformation during the fracture process in the DENT test are much smaller than LDPE. As a result, the new mechanistic approach cannot be applied to UHMWPE. Also, data for the specific work of fracture do not show a linear relationship with l_0, the original EWF method needs to be modified to be applicable to UHMWPE.

In this chapter, conditions for mechanical tests and the description of the trend line revealed by the test results will first be presented. After that, a modified EWF method will be introduced.

3.2 Experimental details

3.2.1 Materials

Ultra-high-molecular-weight polyethylene (UHMWPE) is unique in polyethylene family in that it consists of molecules of extremely long chains. The molecular weight is usually in the order of millions (between 2 and 6 million). UHMWPE is a very tough material because the longer chain serves effective means to transfer load to the polymer backbone and strengthen intermolecular interactions. Like other polymers in the polyethylene family, UHMWPE is inert to most chemicals, except strong oxidizing acids. Furthermore, its impact resistance is highest among all thermoplastics available at present and its moisture absorption lowest. Its coefficient of friction is known to be comparable to that of polytetrafluoroethylene (PTFE), but UHMWPE has better abrasion resistance. Besides, it is tasteless, odorless, and nontoxic.

UHMWPE is a type of polyolefin of which the chemical structure in the backbone chain is shown in Fig. 3-3. It derives its strength largely from the length of individual molecular chains.

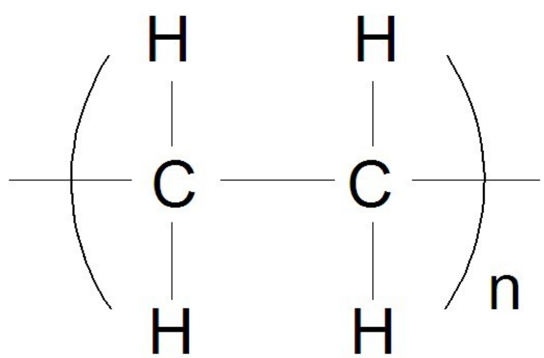

Fig.3-3 Schematic of UHMWPE, with n larger than 100,000.

Although melting temperature of UHMWPE is around 144 to 152 °C, its fiber form should not be used above 80 to 100 °C for a long period of time. It has good ductility at room temperature, but becomes brittle below −150 °C.

Based on all of the above features, UHMWPE is widely used in medical applications like artificial joint, outdoor sports like skis and skating, and also in manufacturing of PVC (vinyl) windows, doors, etc.

In this study, UHMWPE panels are provided by King Plastic Corporation, which has density of 0.973 g/mm^3.

3.2.2 Test set-up

Galbadini Quasar 100 universal testing machine was used to conduct double-edge-notched tensile (DENT) tests at a cross-head speed of 5 mm/min. A Nikon D-70 camera was used to record the deformation and fracture behavior during the whole fracture process at a rate of one photo per ten seconds. These photos were then used to measure the ligament length, in order to determine the crack growth speed during the fracture process.

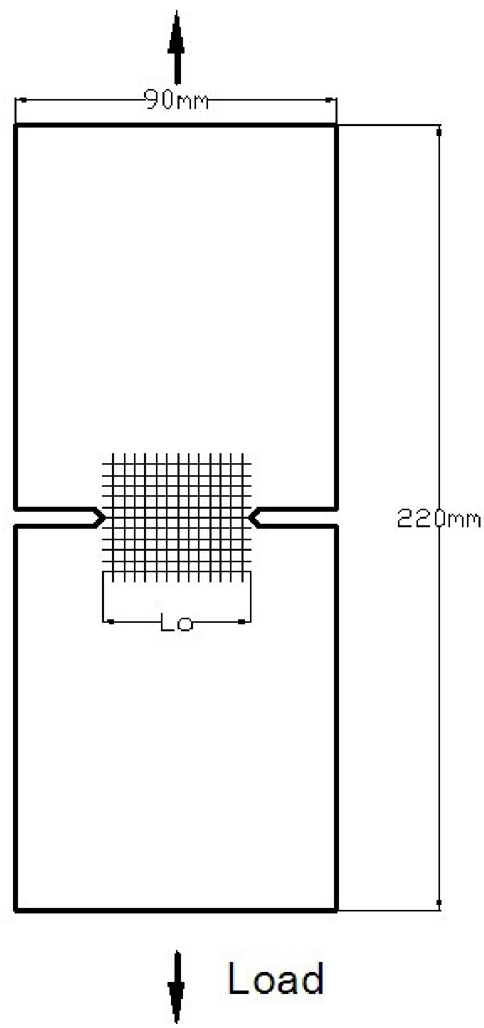

Fig.3-4 Schematic description of DENT specimens and mesh pattern introduced in the ligament section.

As shown in Fig. 3-4, dimensions of the specimens in the DENT tests are 220 × 90 mm^2 with the nominal thickness 6.5 mm. Note that a rectangular mesh pattern was introduced in the ligament area of all specimens before the test, to serve as reference for photographs, taken during the test in order to measure the ligament contraction due to the deformation.

Following the specification given in Equation (3-4), the original ligament length (l_0) of specimens used in this study is in the range from 19 to 31 mm at an increment of 3 mm. Three specimens were tested for each ligament length. To avoid a blunt notch tip to inflate the energy consumption [16], a very sharp tip was introduced prior to the tests using a fresh razor blade. Note that l_0 was measured between the two sharp tips in each specimen using software PHOTOSHOP based on the front view of the photos.

3.3 Deformation and fracture behavior of UHMWPE in DENT test

As discussed in Chapter 2, polyethylene like LDPE can generate extensive necking in the plane-stress fracture, and the necking process consists of two stages: neck initiation and neck propagation, but UHMWPE behaves in a different way. In Fig. 3-5, we can observe that before the maximum load, the load goes up continuously with the increase of the cross-head displacement. After the maximum load, necking is not initiated, thus transition does not exist between necked and un-necked regions. Also crack growth after the maximum load is accompanied with the reduction of ligament thickness, but the extent is not as significant as in LDPE or HDPE.

Since the fracture behavior is different from that shown in LDPE or HDPE, the approach presented in Chapter 2 is not applicable to UHMWPE. Therefore, the formulations of traditional EWF method were used first to check its feasibility for determining the fracture toughness.

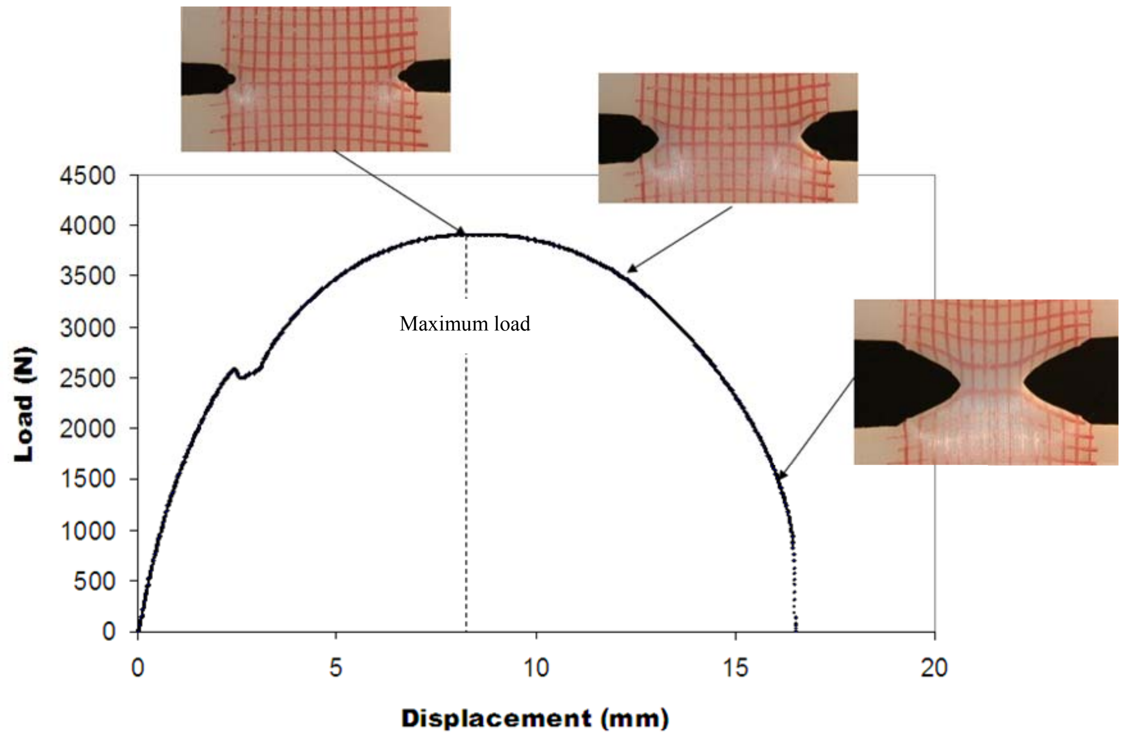

Fig.3-5 Load-displacement curve ($l_0 = 28$ mm) from DENT tests of UHMWPE.

To illustrate the deformation and fracture behavior of UHMWPE in DENT test, a typical load-displacement curve and snap shots of the deformation behavior for specimens used in this study are presented in Fig. 3-5. The figure shows a continuous change of the loading rate before and after the maximum loading point which is marked by a vertical dashed line. In this curve ($l_0 = 28$ mm) we can observe clearly that after the maximum loading point, the load and displacement do not follow a linear relationship. At the very end of the test, prior to the final fracture, a relatively sharp load drop occurs.

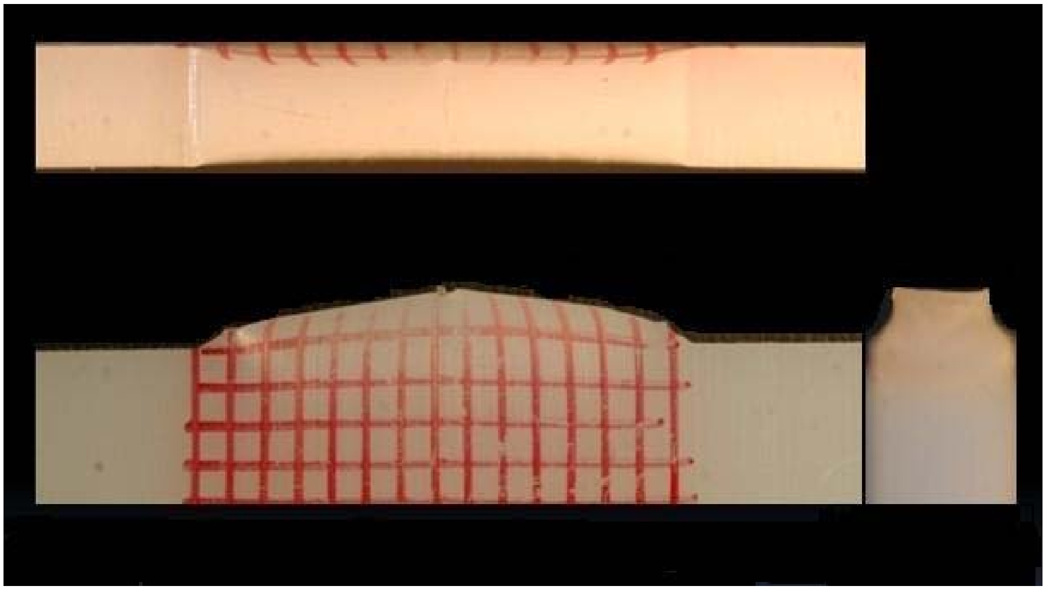

Fig.3-6 Top, front and side views of a DENT specimen (l_0 = 28 mm) after the test.

Fig. 3-6 shows the top, side and front views of a typical specimen after the DENT test. The top view indicates the gentle reduction of thickness from the notch tips to the centre of the ligament. The thickness change will later be approximated by a second order polynomial function of ligament length. The front view of the specimen shows that the mesh line does not maintain straight during the fracture process, suggesting that shear plastic deformation is involved. But compared to LDPE and HDPE, the shear plastic deformation in UHMWPE is not as significant, therefore, to be ignored in the following analysis.

3.3.1 Crack growth speed

Crack growth speed of UHMWPE was found to vary during the test. It is understood as a result of the thickness reduction during the fracture process. Note that for other types of polyethylene like LDPE and HDPE, the thickness remained constant during the neck propagation stage, so was the crack growth speed.

A typical plot of ligament length versus time for UHMWPE is shown is Fig. 3-7, in which time is set to be zero at the commencement of the test. The figure indicates that the rate of ligament length change before the maximum loading point is significantly lower than after the maximum loading point. However, as to be shown later, the crack growth speed is not needed for determining the w_e value in the original EWF method. However, it is presented here as one parameter to obtain an approximation of the total energy used for the plastic deformation based on the new formulation of energy balance equation, as to be discussed later.

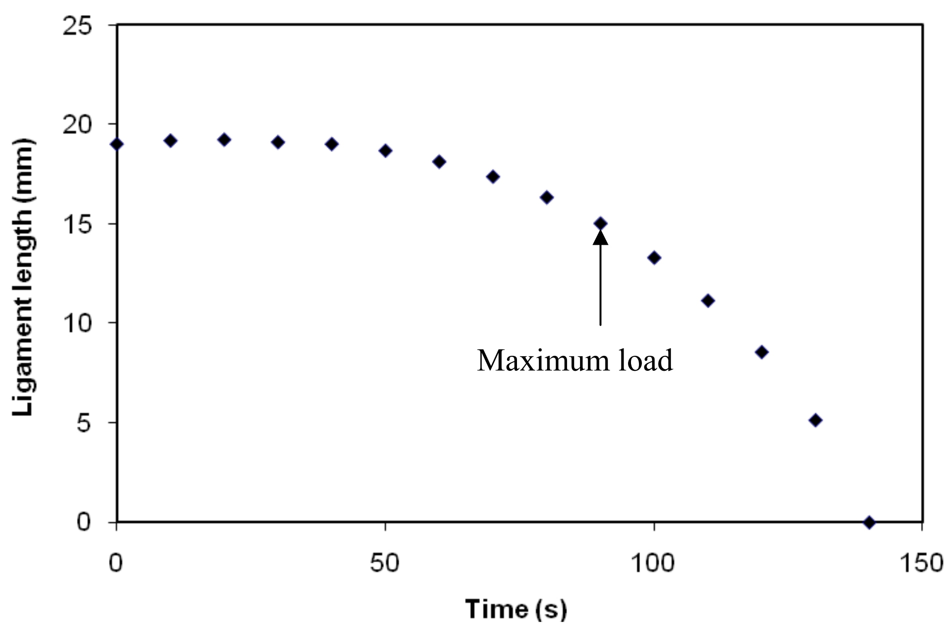

Fig.3-7 Measurement of ligament length (l_0=19 mm) as a function of time during the DENT test.

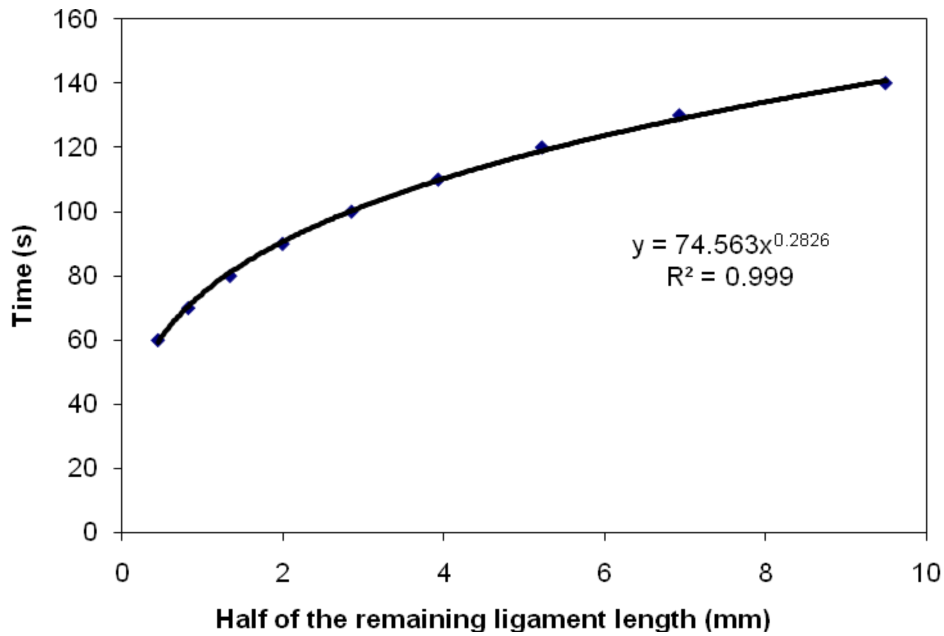

Fig.3-8 Measurement of crack growth during DENT test: a typical plot of half of the remaining ligament length versus time (l_0=19 mm). (Note that some points were ignored at the beginning in order to form the trend line, otherwise, the equation cannot be obtained.)

Fig. 3-8 shows clearly that the relationship between the ligament length and time is not linear, of which the trend line can be approximated using a power law function. Table 3-1 is the summary of the exponent of the trend line for all specimens, from which we can see that the mean value of the exponent is around 0.27.

Table 3-1 The average of the exponent of the governing equations for different ligament length.

Original ligament length l_0 (mm)	Average exponent
16	0.26
19	0.27
22	0.27
25	0.25
28	0.28
31	0.30

3.3.2 Stress-strain relationship from tensile test

A typical time function of the loading curve from the simple tensile test is presented in Fig. 3-9. The corresponding true stress-strain curve is shown in Fig. 3-10. Also a curve that fits the experimental data at the beginning of the stress-strain curve is included in Fig. 3-10, for determining modulus that is used to calculate the energy consumed for unit volume (*U*).

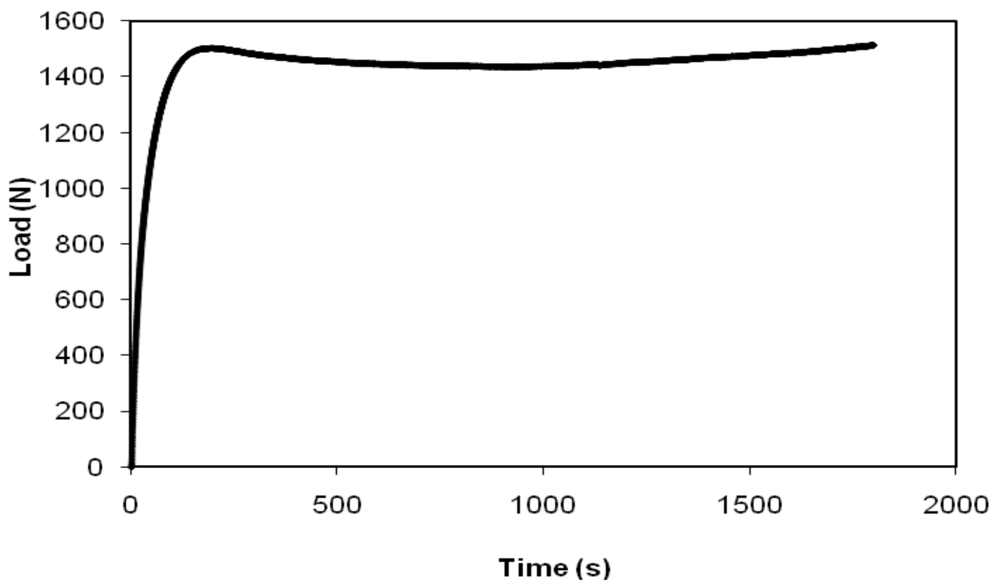

Fig.3-9 Typical tensile test results for UHMWPE: load versus time.

Note that UHMWPE did not show a clear neck front during the tensile test. The deformation is uniform along the whole gauge section of the specimen. At the end of the curve in Fig. 3-9, we can see that the load rises slightly, probably because the deformation starts at both ends of the specimen which are wider than the gauge section. Since there is no significant change in the deformation stage during the test (for LDPE, however, there is a clear transition boundary between neck initiation and neck propagation), the load drop after the maximum point in Fig. 3-9 is much smaller than that in LDPE.

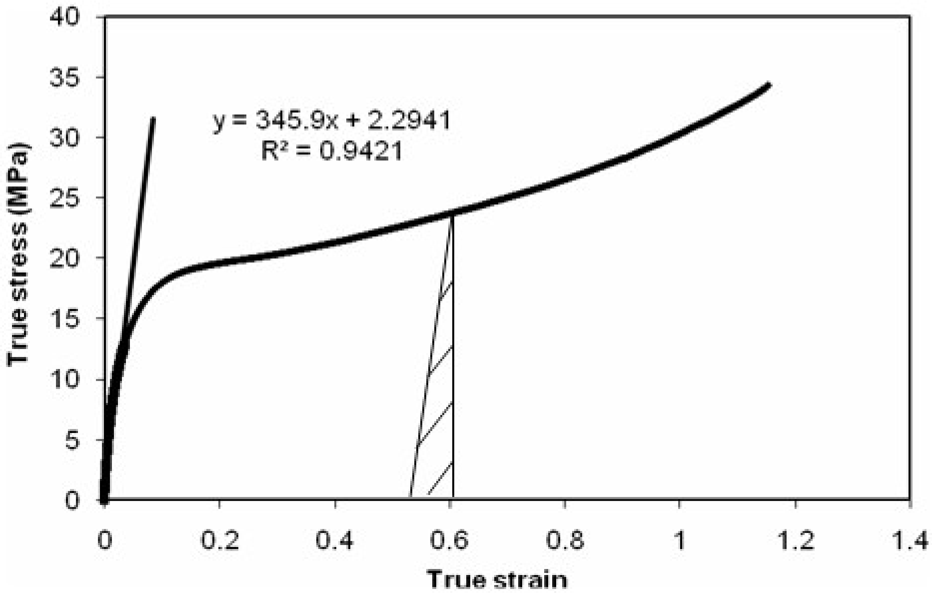

Fig.3-10 Typical tensile test results for UHMWPE: true stress-strain curve.

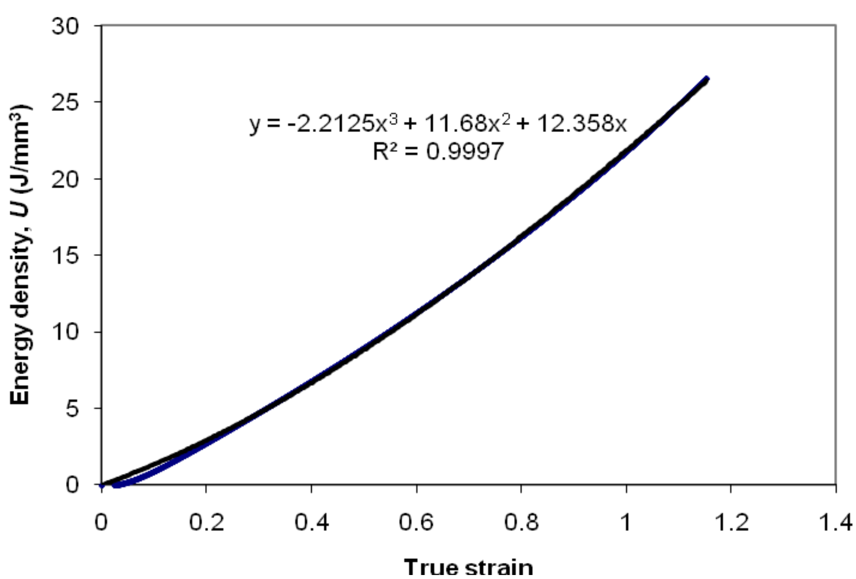

Fig.3-11 Typical tensile test results for UHMWPE: energy density versus true strain.

The energy density U in Fig. 3-11 was determined from the curve in Fig. 3-10 which represents the area under the stress-strain curve subtracting the elastic energy stored in the specimen (shaded part in Fig. 3-10). In addition, the curve of U versus strain is fitted by a third-order polynomial, based on the nature of non-linear stress-strain curve.

3.4 The new approach and formulation of energy balance equation

To simulate the fracture behavior of the specimens in DENT test, the original ligament region that later undergoes plastic deformation is divided into strips as shown in Fig. 3-12, where H_0 is height and l_0 the original ligament length of the DENT specimen.

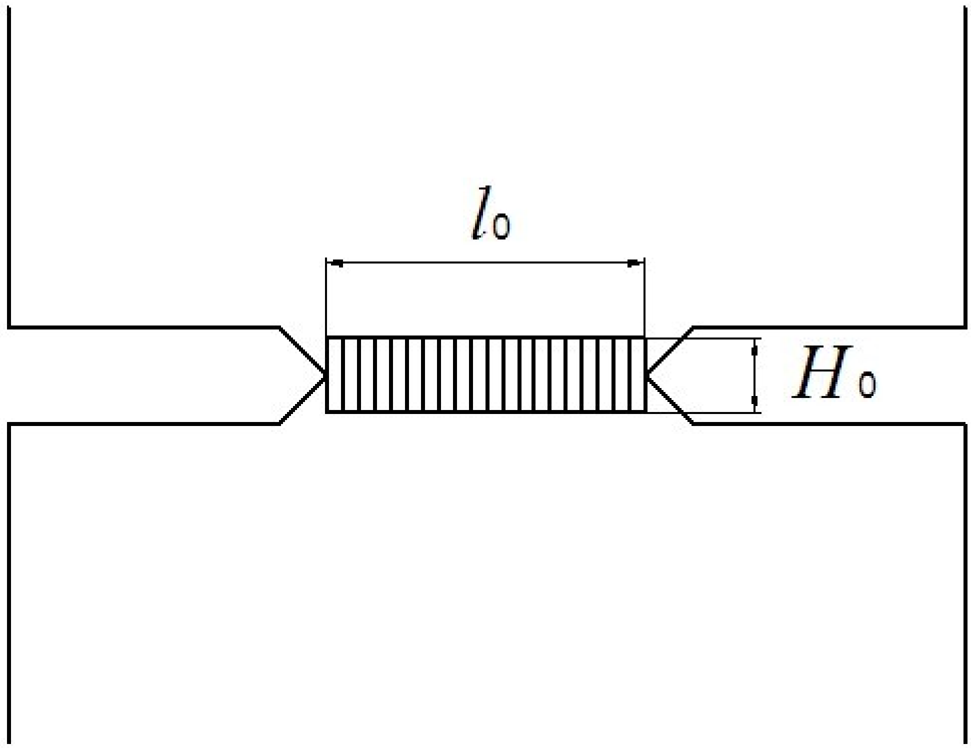

Fig.3-12 The original zone that undergoes plastic deformation during the DENT test.

It is assumed that at the beginning of the test, height of this region H_0 is constant, i.e. a rectangular shape. After the specimen was fully fractured, its shape turns to elliptical, as shown in Fig. 3-13.

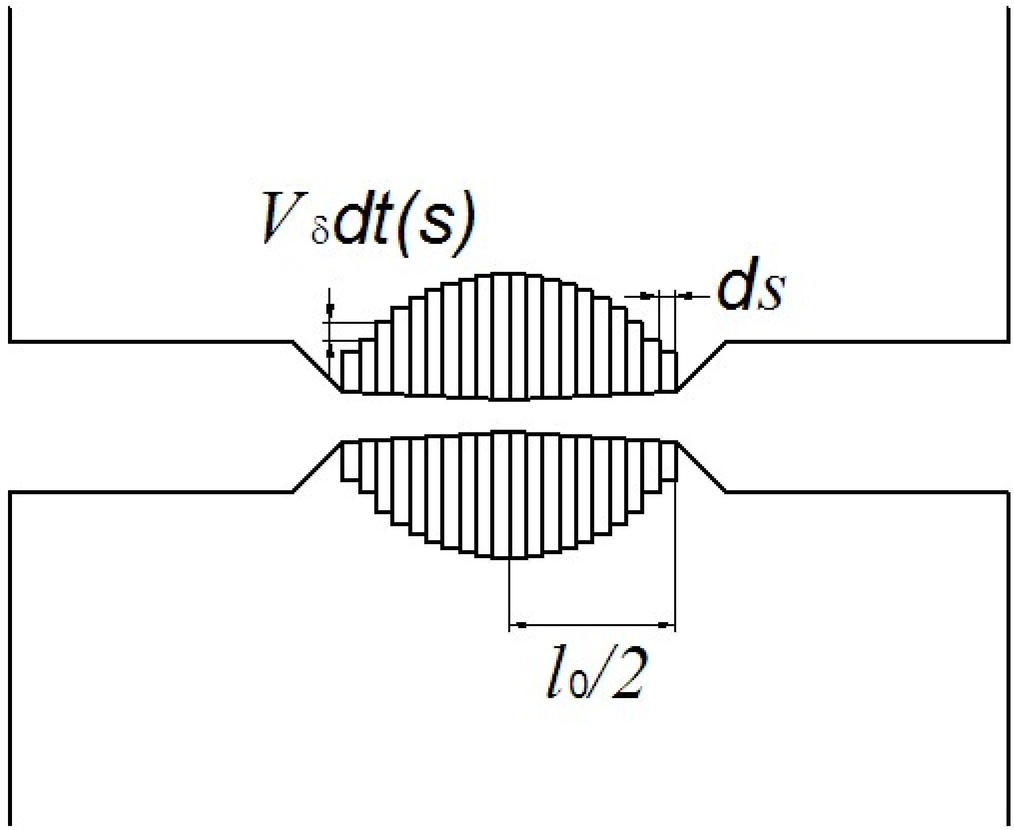

Fig.3-13 The assumed shape of the original zone that undergoes plastic deformation during the DENT test.

As shown in Fig. 3-12, the ligament region is divided into many small rectangular strips with width *ds*. As suggested in Fig. 3-8, time consumed for deformation in each rectangular strip does not have a linear relationship with the strip position, therefore, difference in the height of adjacent rectangular strip should be the product of the cross-head speed V_δ multiplied by the time increment *dt(s)* for the crack growth through the prior strip.

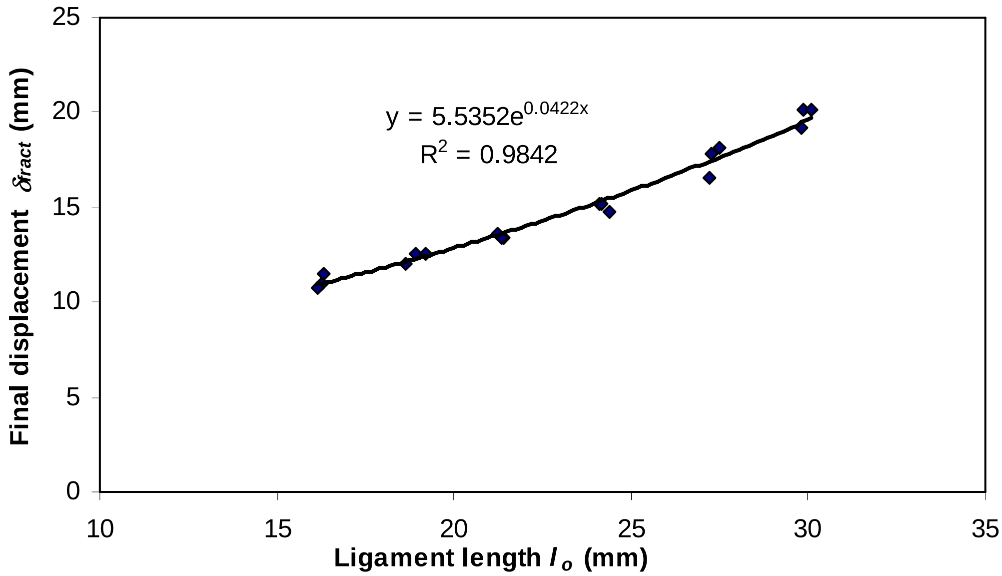

Fig.3-14 DENT test result: plot of original ligament length versus the displacement for fracture (δ_{fract}).

To determine value of H_0 in Fig. 3-12, the final displacement is plotted as a function of the original ligament length in Fig. 3-14. Also, a trend line is used to fit all data. The height H_0 is chosen to be the interception of the trend line to y-axis in Fig. 3-14, i.e. $H_0 = 5.54$ mm.

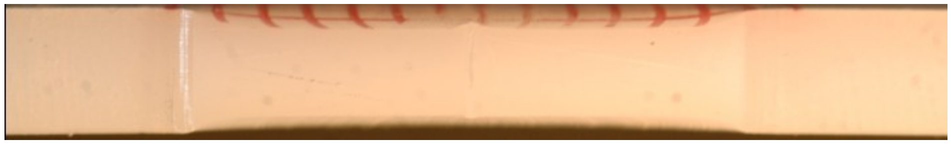

(a)

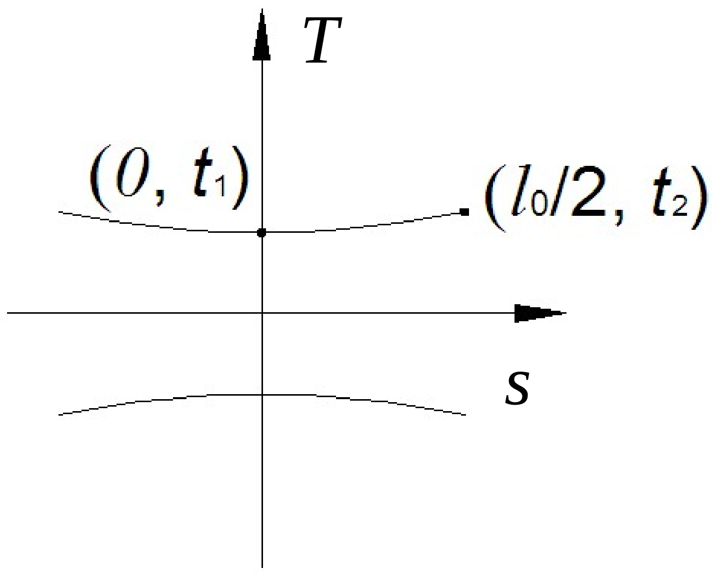

(b)

Fig.3-15 Thickness variation of a post-fractured specimen after DENT test: (a) the top view of the specimen, and (b) second order polynomial function to approximate the thickness variation.

It can be found from Fig. 3-15 (a) that thickness varies along the ligament, which has the narrowest part at the middle. Given that the thickness at both ends of the ligament section is $2t_2$ and in the middle $2t_1$, a second-order polynomial is used to approximate the thickness change.

The second order polynomial function can be written as Equation (3-6), with constants a and b determined using half thickness t_1 and t_2.

$$T = 2as^2 + 2b \tag{3-6}$$

where T is the specimen thickness when half of the remaining ligament length is s.

As shown in Fig. 3-13, height for each small element in the original plastic zone is the original height plus the elongation in the cross-head movement direction:

$$H = H_0 + V_\delta t(s) \tag{3-7}$$

where $t(s)$ is the time as a function of s.

Based on Fig. 3-11b the equation for the relationship between the strain energy density U and true strain can be expressed by Equation (3-8), where the constants c = -2.2125, d = 11.68 and e = 12.358.

$$U = c\varepsilon^3 + d\varepsilon^2 + e\varepsilon \tag{3-8}$$

True strain, based on the definition, is equal to the logarithmic value of the final length divided by the original length in the loading direction, or with the volume conservation during the deformation, equal to the logarithmic value of the original cross-sectional area divided by the final cross-sectional area, i.e. product of width w and thickness t.

$$\varepsilon = \ln\frac{L}{L_0} = \ln\frac{A_0}{A} = \ln\frac{w_0 t_0}{wt} \tag{3-9}$$

where L_0 , A_0 , w_0 and t_0 are original length, area, width and thickness of the specimen, respectively. Accordingly, L, A, w and t are length, area, width and thickness, respectively, of the specimen after the tensile test.

Here, we assume that the ratio of width is proportional to that of thickness, as shown by Equation (3-10):

$$\frac{w_0}{w} = k\frac{t_0}{t} \tag{3-10}$$

where k is the proportionality factor due to the rectangular cross section in the ligament region, and should be smaller than 1 as w_0 is larger than t_0. With the above relationship between width and thickness changes, strain can be expressed as:

$$\varepsilon = \ln k + 2\ln\frac{t_0}{t} \tag{3-11}$$

By ignoring the term (ln k) to simplify the analysis, the expression for strain is given below, though it yields slight overestimate of the strain value.

$$\varepsilon = 2\ \ln\frac{t_0}{t} \tag{3-12}$$

As a result of the strain overestimate, total energy for plastic deformation by stretching, based on the above strain definition, will be overestimated. The overestimate will later be reflected in the curve fitting process, causing the requirement of subtraction of the calculated value in order to fit into a power-law function.

With the strain determined from the dimensional change of the cross section, the energy used in the DENT test for the plastic deformation can be expressed as the energy consumed per unit volume, U, integrated through the whole volume. Since the deformation is symmetrical, the total plastic deformation energy Eu is twice of the integration of U from the middle point to the edge of the ligament (0 to $l_0/2$).

$$Eu = 2\int_0^{\frac{l_0}{2}} H \cdot T \cdot U ds \tag{3-13}$$

After replacing *T*, *H* and *U* by Equations (3-6), (3-7) and (3-8), respectively, the following expression is obtained.

$$Eu = 2\int_0^{\frac{l_0}{2}} (H_0 + V_\delta t(s))(2al^2 + 2b)(c(2\ln\frac{t_0}{2as^2+2b})^3 + d(2\ln\frac{t_0}{2as^2+2b})^2 + e(2\ln\frac{t_0}{2as^2+2b}))ds$$

(3-14)

Table 3-2 Average of the calculated results from Equation (3-14) for all specimens used in this study.

Original ligament length l_0 (mm)	Average results of Eqn. 3-14(Nmm)
16	8525
19	7850
22	9345
25	11681
28	16332
31	20541

The results calculated from Equation (3-14) are listed in Table 3-2 and presented in Fig. 3-16. It can be found that with the increase of the original ligament length the energy goes up accordingly. But the relationship between the two parameters is not linear, as to be discussed in the next section.

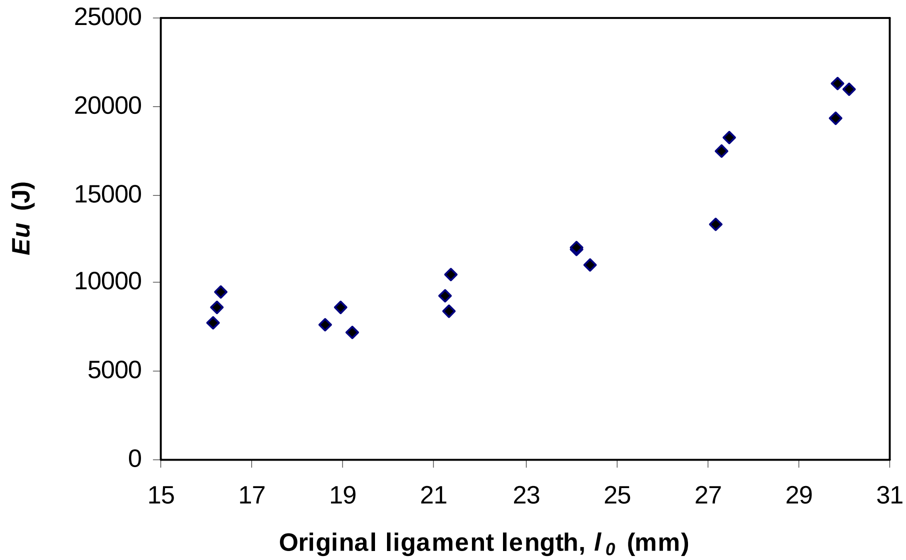

Fig.3-16 Plot of *Eu*, calculated from Equation (3-14), versus the original ligament length.

3.5 Results and Discussion

3.5.1 DENT test results

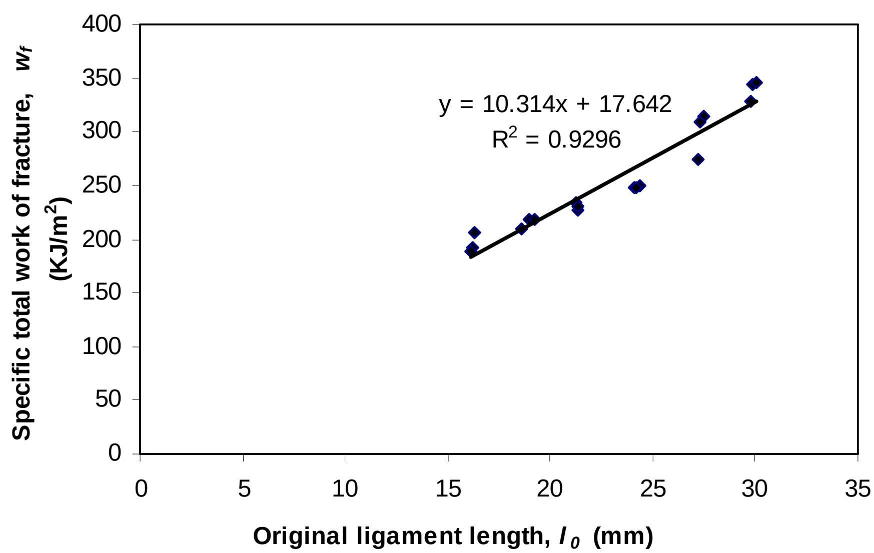

Fig.3-16 The experimental data fitting using the original EWF method.

The original EWF method (based on linear regression) was applied to obtain the results shown in Fig. 3-17, from which w_e is the essential part of total energy which can be determined by the intercept on the vertical axis. The result in Fig. 3-17 seems to follow a linear trend line, but by dividing it into four subgroups according to the original ligament length as shown in Fig. 3-18, the corresponding slope and w_e values listed in Table 3-3 changed dramatically. If all the data follow a linear trend line, the subset should also follow a similar relationship. Therefore, it is clear that the data do not follow a linear relationship.

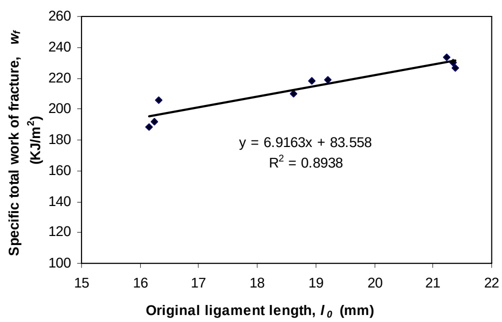

Group 1

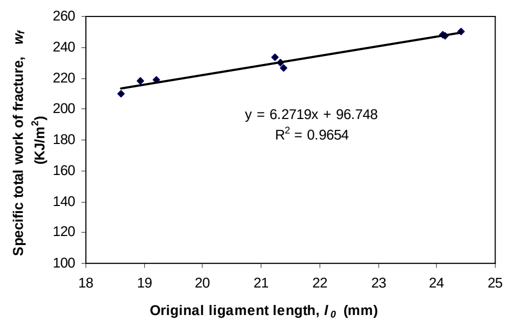

Group 2

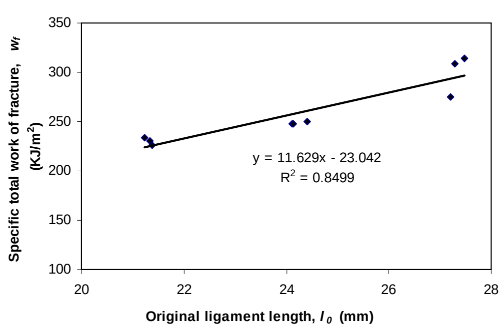

Group 3

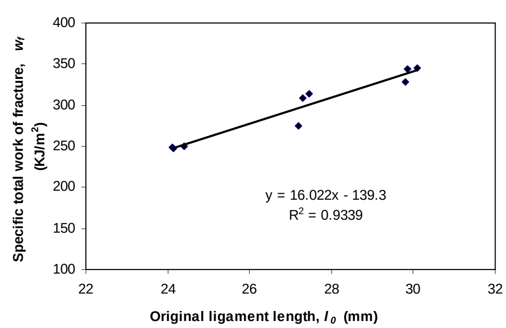

Group4

Fig.3-17 The experimental data fitting for each subset of all the data.

Table 3-3 The slope and w_e values based on the data fitting in Fig. 3-18.

Group	Slope	w_e (KJ/m^2)
1	6.91	83.5
2	6.27	96.7
3	11.63	-23.0
4	16.02	-139.3

To support the argument before, the result of LDPE is also analyzed in the same manner as a comparison. Results for LDPE are divided into four groups based on Fig. 3-19. By taking away any group, the slope and w_e value do not change much as shown in Table 3-4. In this case it is clear that the experimental data follow a linear relationship. Therefore, the original EWF method cannot be applied to UHMWPE.

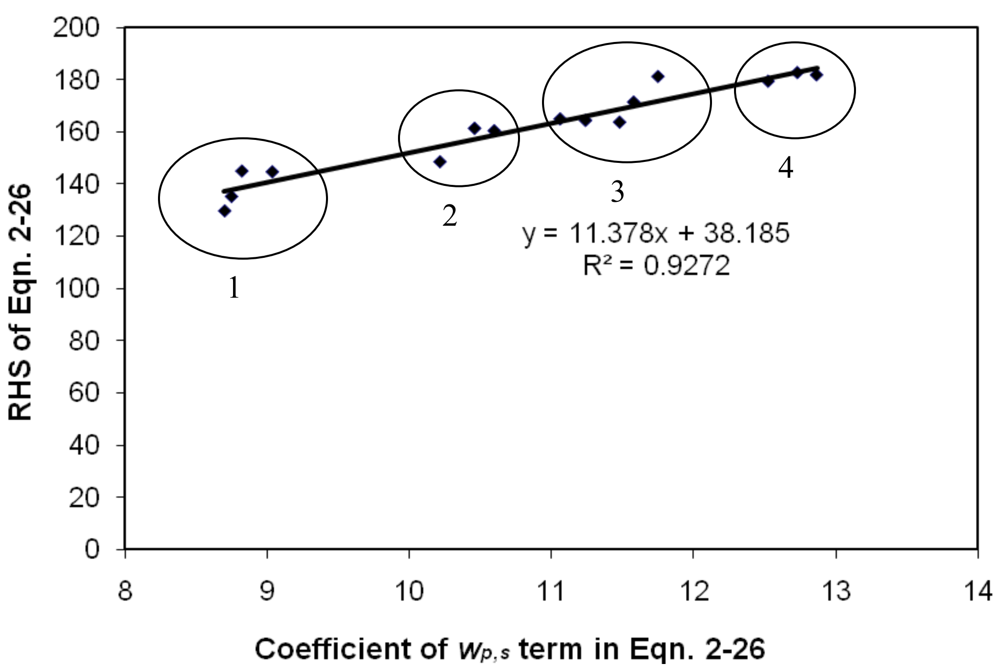

Fig.3-18 Schematic diagram showing how to divide the result of LDPE into small groups.

Table 3-4 The slope and w_e values by taking away each group in Fig. 3-19.

Group	Slope	w_e (KJ/m^2)
1	11.2	40.02
2	11.3	38.86
3	11.5	37.09
4	11.2	39.78

3.5.2 Discussion on the material property

In order to determine the best governing equation to fit all data, an initial value is needed in advance. In this study, assuming that data scattering is not the main resource of error for the curve fitting, the correlation coefficient R^2 can be used as the criterion to evaluate quality of the curve fitting. By subtracting an initial value from all data, it was found that the maximum R^2 value is 0.9587, as indicated in Fig. 3-19. Details of variation of R^2 with the change of w_e can be found in the appendix. Using this approach, the initial value of w_e was found to be 154 KJ/m^2, and the governing equation that includes both the essential part (the initial w_e value) and the non-essential parts (from Fig. 3-19) is:

$$w_f = 154 + 0.0488 l_0^{2.41} \quad (3\text{-}15)$$

Equation (3-15) suggests that the non-essential part, with the power of 2.41, does not follow a straight line with respect to l_0, which is different from the expression in the original EWF method.

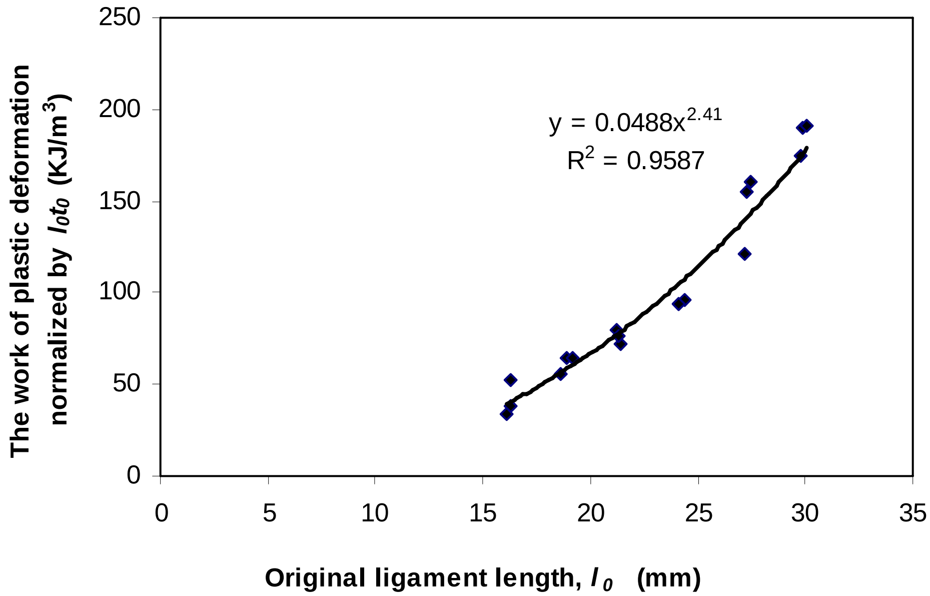

Fig.3-19 Regression plot of the plastic deformation energy versus the original ligament length.

3.6 Conclusions

The fracture behavior of UHMWPE is different from LDPE and HDPE. It was found that no significant necking or shear plastic deformation occurs during the fracture process in the DENT test. The study also shows that the original EWF method was not applicable to UHMWPE, as the data of specific essential work of fracture do not show a linear function of l_0.

To justify the results from the modified EWF method, a new approach was introduced to calculate the energy consumption for the plastic deformation, based on the energy density obtained from simple tensile test and the a rectangular zone for plastic deformation in the DENT test. It was found that the exponent of the trend line for the plastic deformation energy consumption is not 1.

References

[1] Broberg KB. Critical review of some theories in fracture mechanics. Int J Fracture 1968; 4:11-8.

[2] Broberg KB. Crack–growth criteria and non-linear fracture mechanics. J Mech Phys Solids 1971;19:407-18.

[3] Briberg KB. On stable crack growth. J Mech Phys Solids 1975; 23: 215-37.

[4] Cotterell B, Reddel JK. The essential work of plane stress ductile fracture. J Int Fract 1977; 13: 267-277.

[5] Mai YW, Cotterell B. The essential work for tearing of ductile metals. Int J Fracture 1984; 24: 229-36.

[6] Mai Y-W, Wong S-C, Chen X-H. Application of fracture mechanics for characterization of toughness of polymer blends. In: Paul DR, Bucknall CB, editors. Polymer blends: formulations and performance, Vol 2. NewYork: Wiley; 2000. P. 17-58.

[7] Mai YW, Cotterell B. On the essential work of ductile fracture in polymers. Int J Fracture 1986; 32: 105-25.

[8] Mai YW, Powell P. Essential work of fracture and J-integral measurements for ductile polymers. J Polym Sci Part B Polum Phys 1991; 29: 785-93.

[9] Mai YW, Cotterell B, Horlyck R, Vigna G. The essential work of plane stress ductile fracture of linear polyethylenes. Polym Engng Sci 1987; 27(11):804-9

[10] Peres F, Schon C. Application of the essential work of fracture method in ranking the performance in service of high-density polyethylene resins employed in pressure pipes. J Mater Sci 2008; 43(6): 1844-50.

[11] Kwon HJ, Jar PYB. Application of essential work of fracture concept to toughness characterization of high-density polyethylene. Polym Engng Sci 2007; 47(9): 804-9.

[12] Maspoch ML, Ferrer D, Gordillo A. Effect of the specimen dimensions and the test speed on the fracture toughness of iPP by the essential work of fracture (EWF) method. J Appl Polym Sci 1999; 73(2): 177-87.

[13] Hashemi S. Determination of the fracture toughness of polyethylene terephthalate (PBT) film by the essential work method: effect of specimen size and geometry. Polym Engng Sci 2000; 40(3): 798-808.

[14] Levita G, Parisi L, Marchetti A. Effect of thickness on the specific essential work of fracture of rigid PVC. Polym Engng Sci 1996; 36(20): 2534-41.

[15] Hashemi S. Work of fracture of PBT/PC blend: effect of specimen size, geometry, and rate of testing. Polym Engng Sci 1997; 37(5): 912-21.

[16] Williams JG, Rink M. The standardization of the EWF test. Engng Fract Mech 2007; 74(7): 1009-7.

Chapter 4 Conclusions

A mechanistic approach has been successfully applied to characterization of LDPE for its fracture behavior in DENT test. Similarly to HDPE, fracture of LDPE involves neck initiation and neck propagation. Observations during the test suggest that plane-stress fracture only occurs at the neck propagation stage. During this stage, three mechanisms, i.e. fracture surface formation, shear plastic deformation and neck growth were observed. Specific energy densities for the three mechanisms were determined using a linear regression method.

Fracture resistance, in terms of w_e, can be compared directly with those based on the original EWF concept. Difference was found to be small between the w_e values determined from different methods for the LDPE used in the study. Test results suggest that the original EWF method is invalid for DENT test of LDPE, especially when the fracture behavior is accompanied by large deformation and necking. Specific energy for necking in a simple tensile test was determined. It was found that the necking energy density from DENT test using the new mechanistic approach is close to that from the simple tensile test. This provides some support to the validity of the new mechanistic approach for characterizing the plane-stress fracture behavior of LDPE.

For UHMWPE, however, it was found the necking and shear plastic deformation during the fracture process in the DENT test is not as significant as LDPE. Since data for the specific work of fracture do not show a linear relationship with l_0, the original EWF method is not applicable to UHMWPE. Instead, the original EWF method was modified using a power law function.

A new approach and formulation of energy balance was introduced to justify the results from the modified EWF method. It was found that the trend line for the energy consumption for the plastic deformation does not follow a linear relationship, based on simple tensile test results. That means original EWF method cannot be applied to characterize fracture toughness of UHMWPE.

For the study conducted here, the following recommendations are proposed for the future studies.

(i) For LDPE, the inconsistent loading-unloading behavior has caused uncertainty of the stiffness. As a result, difference between Equations (2-24a) and (2-25) is significant. At this stage, reason for its occurrence is not clear. It is suggested that the future study should be conducted to understand this behavior, to elucidate its relationship with the change of molecular structure during the loading-unloading test. In addition, this study is based on test at ambient temperature, thickness, etc. Future study should include influence of those parameters on the test results.

(ii) For UHMWPE, not all fracture mechanisms, such as shear plastic deformation, are considered in the formulation of the energy balance equation, since it does not cause any significant discrepancy between the calculated results and the experimental data for the exponent for the power-law function of the plastic deformation energy. In the future study, the shear plastic deformation and the thickness change along the loading direction should be considered in the analysis, to further improve accuracy of the prediction.

Appendix

To determine the initial w_e value in Equation (3-14), variation of the correlation coefficient R^2 with the change of w_e value was established, as shown in Fig. A-1. Based on the figure, w_e value is determined to be the one that yields the maximum R^2, which is equal to 154 KJ/m^2.

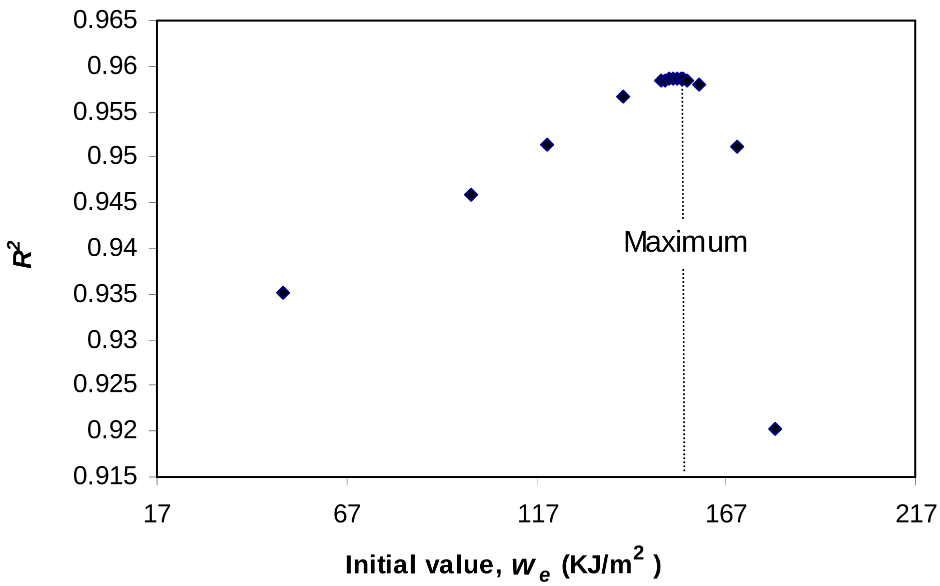

Fig. A-1 Variation of R^2 with the change of w_e value.